FOREST STRESS ANALYSIS IN HONG KONG'S FORESTED WATER CATCHMENTS USING SATELLITE-BASED FLUORESCENCE

SYED MUHAMMAD IRTEZA

PhD

The Hong Kong Polytechnic University

2021

The Hong Kong Polytechnic University

Department of Land Surveying and Geo-Informatics

Forest stress analysis in Hong Kong's forested water catchments using satellite-based fluorescence

Syed Muhammad Irteza

A thesis submitted in partial fulfillment of the requirements for the degree of Doctor of Philosophy

January 2019

CERTIFICATION OF ORIGINALITY

I hereby declare that this thesis is my own work and that, to the best of my knowledge and belief, it reproduces no material previously published or written, nor material that has been accepted for the award of any other degree or diploma, except where due acknowledgement has been made in the text.

_____ (Signed)

SYED MUHAMMAD IRTEZA ____(Name of Student)

ABSTRACT

Measurement of Sun-induced Chlorophyll Fluorescence (SIF) from a vegetation canopy, gives insight into physiological perturbations that might cause stress in vegetation. Because it can indirectly measure photochemical processes and carbon sequestration within the vegetation, SIF can be used as an early indicator of plant stress, and hence is a reliable tool to monitor overall vegetation health. Plants emit Fluorescence from Chlorophyll-a which is present in plant leaves, in the form of an electromagnetic signal, when they are exposed to light. However, SIF is only a small fraction, (approximately 1-2%) of total radiation emitted by green plant leaves. The emission spectrum of fluorescence peaks at two broadband spectral regions which are centered at 685 nm (Red) and 740 nm (Far-Red). Recently the scientific community has shown great interest in satellite-based monitoring of plant physiological and environmental changes by the detection of SIF, and several methodologies have been developed to assess the factors that contribute to plant stress. The main aim of this research is to calculate the SIF quantitatively using available hyperspectral satellite imagery as well as field-based spectrometers over Hong Kong's vegetated areas, in order to assess the vegetative health of the region and recommend the best SIF measurement methodology. In this study fluorescence is estimated from Hyperion satellite images, in the atmospheric absorption band O_2A (far red wavelengths) around ~760 nm.

Field surveys were conducted from May 2015 to September 2018 by using portable hyperspectral and multispectral sensors in three different structural classes of vegetation (forest, shrubland, and grassland) at Tai Mo Shan in Shing Mun Country Parks, and Kowloon reservoir. The field plan was developed while considering cloud conditions,

seasonality of vegetation, and satellite overpass. Vegetation spectra were collected over different seasons at sample points dispersed in the study area. Field samples were also obtained at morning and evening times, as well as over the whole day at 20-minute intervals. The field data were used to relate ground observations with satellite observations. On-demand satellite data from NASA were also acquired to increase the number of coincident observations. High resolution Planet data were also processed monthly month, to set the field and satellite data in context of seasonal phenological changes in the study area. Two methods of fluorescence retrieval were applied to both satellite data and field data, namely the Barun Method extension FLD-M and the Fraunhofer Line Difference (FLD) method. Fluorescence results were also compared with NDVI, and analysed according to vegetation seasonality, natural vegetation structural classes, exotic plantations and five age groups of forest having median ages of 7, 20, 39, 61,70 years.

Results indicate that the SIF methods are more sensitive to phenological change than NDVI. The SIF methods respond earlier and stronger, to senescence in winter and greening up in summer- which is also useful for monitoring disease in croplands and forests, as early action is needed to combat disease. Diurnal analysis from the field survey spectrometer showed that NDVI seems unresponsive to time of day (morning to evening), whereas both fluorescence methods respond to sunlight intensity - and the FLD method is more sensitive than FLD-M to the changes over the day. Both seasonal and diurnal results indicate that Fluorescence is a much better method than NDVI for measuring subtle changes in vegetation health.

Although the NDVI shows differences between different structural stages of vegetation, with gradual decrease from woody vegetation to grassland, forest and exotic plantations in the study area do not show any significant difference. However, fluorescence shows very significant differences between plantations and forest, and the difference is greater in dry season. FLD-M method showed better separation between plantations and forest than the FLD method Additionally, during the end of greening season (October), the NDVI does not show significant differences between Forest, Open Forest, Shrubland and Open Shrubland, while the FLD method clearly distinguishes between the four woody structural stages of vegetation in the study area. The FLD method shows a continuous and significant increase in fluorescence emission with age up to 61 years, and the old growth forest shows minimum fluorescence. This decrease in photosynthesis for the old growth forest is much greater for the FLD retrieval than for NDVI and FLD-M. This study contributes to understanding of the dynamic functioning of vegetation and photosynthesis mechanisms. It also provides an improved operational remote sensing methodology for scientific investigation of the forest health status of Hong Kong's Country Parks.

Key Words: *Sun Induced Chlorophyll Fluorescence, FLD, Hyperion, hyperspectral remote sensing, vegetation stress, Grassland, Vegetation physiology, chlorophyll fluorescence.*

PUBLICATIONS ARISING FROM THE THESIS

Published Papers

1 **Syed M Irteza**, Janet E Nichol, SHI Wen-zhong John, Sawaid Abbas (2020). "NDVI and fluorescence indicators of seasonal and structural changes in a tropical forest succession". Earth Systems and Environment (ESEV).

2. **Syed M Irteza**, SHI Wen-zhong John, Janet E Nichol, Sawaid Abbas (2020). "Association of NDVI and SIF to Species diversity in a 70-year tropical forest". Journal of Geospatial Engineering.

3. Sawaid Abbas, Janet E. Nichol, Jinlong Zhang, Gunter A Fischer, Man Sing Wong, **Syed M Irteza** (2020). Spatial and environmental constraints on natural forest regeneration. Science of the Total Environment.

4. Abbas, S.; Nichol, J.E.; Fischer, G.A.; Sing, M.; **Irteza, S.M**. Agricultural and Forest Meteorology Impact assessment of a super-typhoon on Hong Kong's secondary vegetation and recommendations for restoration of resilience in the forest succession. Agricultural and Forest Meteorology. 2020, 280, 107784.

Conference Paper

1. **Irteza, S. M**., & Nichol, J. E. (2016). Measurement of Sun Induced Chlorophyll Fluorescence Using Hyperspectral Satellite Imagery, ISPRS - International Archives of the Photogrammetry, Remote Sensing and Spatial Information Sciences, Volume XLI-B8, pp.911-913

ACKNOWLEDGEMENTS

All glory and praise are for Allah, the sustainer of life. All Blessings for the final Prophet Muhammad (Peace be upon him) and his family. My sincerest thanks to many individuals who supported me in many ways and without those it would not be possible to complete this study.

I would like to thank my supervisor and mentor Professor Janet Nichol who guided me and patiently supported me throughout this journey. Her motivation kept me on track all these years. Profound thanks to my Chief Supervisor Professor john Wenzhong Shi for supporting me especially during last two years of my PhD when I came under his supervision. This research would not be possible without the support of the Hong Kong Polytechnic University Scholarship. I would also like to thank Associate Professor Dr Charles for his support during this PhD.

I would like to express my sincere gratitude to my friend and colleague Dr Sawaid Abbas whose constant motivation and support helped me during this journey. I would like to thank all my friends and colleagues specially Dr Majid Nazeer for his decade long friendship and support specially in Hong Kong, Dr Usman, Dr Bilal for giving me memorable time during my studies. I would also like to thank my fellow Hong Kong Polytechnic Colleagues Dr Ivan and Dr Esterina for their friendship, Dr Rashmi, Dr Zeeshan Sattar, Dr Nanette, Dr Waleed, Dr Sachin, Dr Arshad, my roommate Dr Zahoor, Dr Mateen, Shamsa, Sarah, Sidrah, Mr Naeem, Valeria, Dr Imran for their support throughout. Special thanks to Department of Land Surveying and Geo-informatics General Office staff, Technical staff and the supporting staff for their help whenever

needed. I am very thankful for Finance Office and Research Office of The Hong Kong Polytechnic University for their support.

Thanks to few individuals Mr Asif, Mr Asad and Mr Raza whose support in Hong Kong made this journey easier.

Last but not the least I would like to thank all my family members, specially my parents, for patiently waiting for me to come back and my wife Amber who always supported me. A special thanks to my dearest cousin Asad and my younger sister for their constant support. In the end, I would like to give gratitude to my parents whom I loved the most and all my success in life is because of them.

Table of Contents

LIST OF FIGURES

LIST OF TABLES

ABBREVIATIONS

AOD	Aerosol Optical Depth
APAR	Absorbed Photosynthetically Active Radiation
Chl	Chlorophyll
DOAS	Differential Optical Absorption Spectroscopy
ESA	European Space Agency
FLD	Fraunhofer Line Discrimination
FLEX	Fluorescence Explorer
GOSAT	Greenhouse gases Observing Satellite
GPP	Gross Primary Product
LAI	Leaf Area Index
LUE	Light Use Efficiency
MODIS	Moderate Resolution Imaging Spectroradiometer
NDVI	Normalized Difference Vegetation Index
NPP	Net Primary Product
NPQ	Non Photochemical Quenching
OCO-2	Orbiting Carbon Observatory – 2
PAM	Pulse Amplitude Modulated
PAR	Photosynthetically Active Radiation
RTM	Radiative Transfer Models
SFM	Spectral Fitting Method
SIF	Solar Induced Chlorophyll Fluorescence

SNR	Signal to Noise Ratio
SSI	Spectral Sampling Interval
SVD	Singular Vector Decomposition
TOC	Top of Canopy

CHAPTER 1 INTRODUCTION

1.1. Background

Plants convert light energy into chemical energy to make food. When light photons fall on a vegetative surfaces three processes happen. Firstly, photochemical quenching - PQ (Photosynthesis), secondly, non-photochemical quenching (Heat dissipation) and thirdly chlorophyll fluorescence, all as by-products of photosynthesis (Figure 1-1). All these processes are well understood, and laboratory tested through various experiments. It has been established that when the PQ process receives an excess amount of light; it releases the energy in the form of heat or fluorescence to save itself for photoinhibition, and the relationship is somewhat inversely proportional. Several factors contribute to the division of these three energies. Plant physiology and environmental factors such as nutrients, water sources and temperature play a part in the division of this energy. Measuring fluorescence will therefore give an indication of plant stress, as it shows how effectively plant pigments convert the very minute amount of fluorescence energy. The health status of the plant can thus be estimated by the amount of fluorescence it produces.

When radiation of short wavelengths falls on a vegetated surface, the chlorophyll content in the pigments of healthy plants emit certain wavelengths in the range of red and ear-infrared, which is called fluorescence (Baker, 2008). Remote sensing can be utilised to measure fluorescence by examining the narrow bands within the Red and Infrared region, although changes at these wavelengths are very minute. This means that even narrowband hyperspectral sensors may only detect slight changes. However, the advantage of this measurement is not just to improve the understanding of vegetation physiology, but also

to help understand the interplay between plant environmental factors such as soil moisture content, canopy structure and solar azimuth. As this signal is relatively weak compared to other broad-spectrum measurements, detecting it through spaceborne sensors automatically creates challenges for the remote sensing experts.

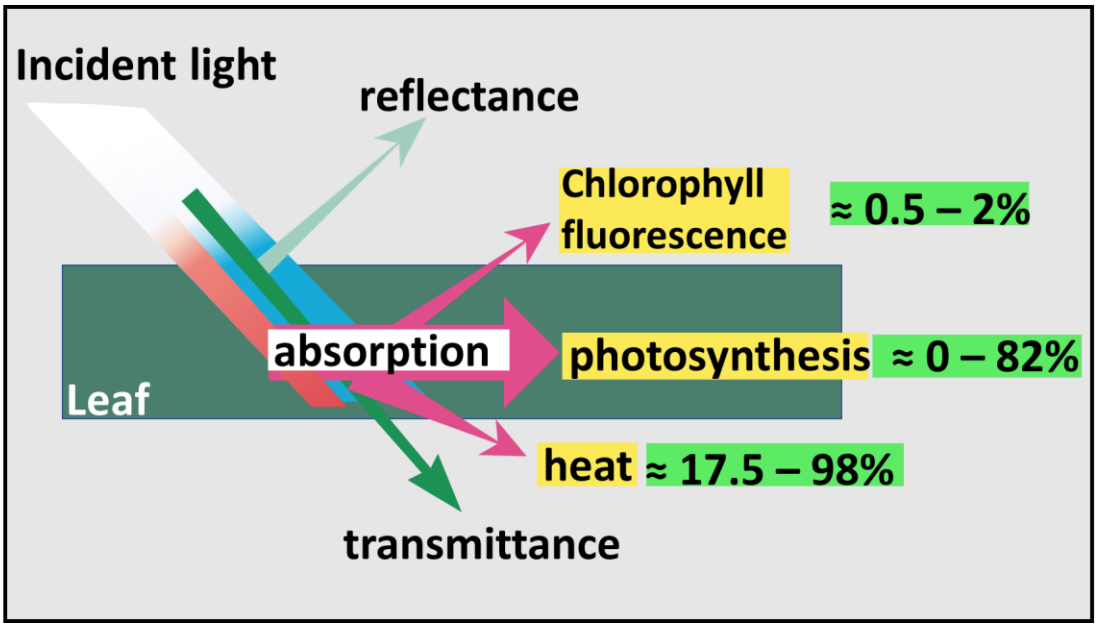

Figure 1-1: Chlorophyll fluorescence is the byproduct of photosynthesis. Only 2 % of the total incoming light is converted to chlorophyll fluorescence, making its retrieval very difficult

(Davidson et al., 2003)

Three absorption bands are present in the solar irradiance spectrum: one in red (656.3 nm) and another two in the near-infrared region (687 nm and 760 nm respectively), which made it possible to quantify sun induced chlorophyll fluorescence (SIF). The red absorption band is due to the Hydrogen Ha, and the infrared absorption bands are due to oxygen absorption.

The SIF emission peak lies near these bands. Therefore, retrieval of fluorescence around these bands under natural sunlight using the Fraunhofer lines infilling method (FLD) is

possible (Plascyk, 1975). Reflectance at 760 nm is 5 to 6 times higher than at 680 nm and 656 nm.

Fraunhofer noticed that at certain wavelengths, gaps between lines of the Solar spectrum drop suddenly. Scientists later called those lines the Oxygen Absorption lines. Due to the presence of oxygen, some of the photons at wavelengths 680 nm and 760 nm show a sharp dip in the solar spectrum (Frankenberg et al., 2013). The O_2B band exists exactly at the 685 nm peak of chlorophyll fluorescence, but its detection is more difficult than for the chlorophyll fluorescence peak at the O_2A band 760 nm, because the O_2B band depth is 70 % lower than the O_2A band. The O_2A band peak does not fully coincide with the chlorophyll fluorescence peak at 760 nm, but it contains 50 % of the absorption peak. Also, the width of the O_2A band is wide enough for deciphering SIF using high spectral sensor (Moya, 2004).

Satellite based measurement of SIF has emerged over the last few years as a new method to globally monitor vegetation status from space (Guanter et al., 2007). First ever map of global fluorescence has been created within this decade as well (Frankenberg et al., 2011; Joiner et al., 2011).

Electromagnetic signals are used to measurement the biophysical process going on inside the plant from airborne and spaceborne equipment. If we can determine which feature has a specific electromagnetic spectrum, we can determine the chemical composition of an object, and. automaticallyanalyze the spatiotemporal distribution and disturbances in vegetation globally and locally. Chlorophyll content in the plant as well as its water content is the good indicator of the biochemical process while biophysical properties such

as Leaf Area Index can give us its biophysical behaviour. Overall, these estimates indicate stress in plants as well as diversity in the overall vegetation.

Terrestrial vegetation photosynthetic activity takes place in the 400 – 700 nm range which in the scientific community is termed Absorbed Photosynthetically Active Radiation (APAR). The relationship between the tree canopy and the radiation is difficult as it depends on many physical functions. The three main functions that drive the relation between solar radiation and the plant itself, and which are widely researched and well understood are absorption, reflection and transmission.

Characteristics of leaf reflectance spectra are defined by

- In the visible region (400 – 700 nm)- chlorophylls are the major receptors of foliar photosynthetic pigments.
- In the infrared region (700 – 1300 nm)- reflectance is determined by the leaf structure.
- In the shortwave region (1300 – 2500 nm)- reflectance is determined by water and protein absorption properties.

The fluorescence signal is very weak compared to other emitted signals and detecting it from space is challenging, as it is only a tiny fraction of reflected solar radiation emitted from the surface. Different solar spectra have been detected by several methods for certain features such as Hα line, which was found to be at 656 nm, the K-I line at about 770 nm (Joiner et al., 2011), In this research most emphasis will be given to two atmospheric absorption spectral regions, namely the O_2A band around 760 nm, and the O_2B band around 687 nm (Guanter et al., 2010). At these particular wavelengths, it is only possible to detect Solar Induced Fluorescence because the original radiation is considerably

reduced, which allows for the sensors to detect the SIF (Meroni et al., 2010). The spaceborne sensor is now widely used for the detection of such radiation. Unfortunately, there is no dedicated satellite for this particular purpose alone. However, different satellite sensors have adequately fine spectral bands , such as the Medium Resolution Imaging Spectrometer (MERIS) sensor of the European Space Agency (Guanter et al., 2007) and the Fourier Transform Spectrometer sensor of the Japanese Greenhouse gases Observing Satellite (GOSAT) platform (Joiner et al., 2011). Fluorescence retrieval methodologies have also been applied to recent satellite sensors such as the Global Ozone Monitoring Instrument 2 (GOMI-2) (Joiner et al., 2013) and the Orbiting Carbon Observatory 2 (OCO-2) (Frankenberg et al., 2012).

Literature review indicates a major gap in the understanding of the fluorescence signal: understanding has been developed over small periods such as from seconds to days, but the overall longer-term relationship between chlorophyll fluorescence and seasonal phonological changes in photosynthesis remains to be fully understood. There is an urgent need to further develop the theory and models to understand these long-term fluorescence functions because it will assist understanding of the intricate working of the global carbon cycle, including global climate change. Robust models should be developed to link the SIF with the GPP to tackle this problem. Many drawbacks in the existing models for the retrieval of fluorescence from space as well as measurements from ground based equipment have been discussed (Niinemets, 2010). Space-based SIF measurement is based on passive Solar induced Chlorophyll fluorescence which has many unsolved problems, and it needs to be solved. The main problem with passive measurements of SIF from space is the availability of a hyperspectral sensor with good spatial and spectral

characteristics. Until August 2018 there was no single space-based platform dedicated to fluorescence retrieval. Satellites like GOSAT, MODIS, and OCO-2 with the help of ground measurements had been used in the fluorescence-based studies.

Although remote sensing of SIF has recently been examined for better understanding of photosynthesis and its response to the environment, , it is the premise of this research, that it remains unclear how SIF and photosynthesis are linked at different spatial scales across the growing season. Additionally , as the Gross Primary Productivity (GPP) of plants depends on whole-season growth, the mechanistic link between GPP and SIF is not completely understood (Migliavacca et al., 2017).

Examination of the different SIF measurement techniques reveals numerous knowledge gaps that require further study at different scales for better and more timely determination of vegetation stress (Alexander et al., 2015). The investigation of Gross Primary Production at global scale still requires an extensive amount of research even after the decades of remote sensing-based studies (Badgley et al., 2017).

1.2. Research objectives

Main objectives of this study are as follows:

- To investigate the SIF measuring capability of hyperspectral satellite sensors and present the most suitable methodology for the Hong Kong region.
- To investigate the relationship between NDVI and SIF.
- To investigate the health of grassland and other vegetation types in Hong Kong's mountainous regions using SIF over different seasons of the year.
- To create a link between field spectrometer and hyperspectral satellite data for SIF retrieval.

1.3. The significance of this study

Accurate retrieval of the fluorescence signal by remote sensors could provide a unique understanding of the global vegetation photosynthesis cycle, especially since SIF is a direct indicator of canopy photosynthesis. This would offer an alternative and new quantitative approach to measure carbon sinks (Coops, 2015). As with all remote sensed vegetation indices, SIF is considered a noninvasive technique (Moya et al., 1995) Along with theories of photosynthesis, SIF theories have been understood and taught in schools, to understand how plants converts solar energy into chemical compounds to make food. However, there are still many gaps in understanding the complexity of how plants balance the total energy received. The importance of plant functioning for human life is attested by the 10 Nobel Prizes which have been awarded for the description of, and unravelling the mystery of, photosynthesis, the most important process on earth for every living organism.

As SIF retrieval from the space-based platforms is a passive and non-invasive technique it can be applied in precision farming, managing forests and estimating terrestrial carbon budgets. It has been found that different species have different fluoresce emissions (Rossini et al., 2014) and this can be useful in measuring the stress of different vegetative species where the NDVI tends to saturate especially in dense canopies and at high biomass levels (Brantley et al., 2011).

Vegetation monitoring plays a key role in monitoring the global carbon cycle. There are several missions which carry out global vegetation monitoring, using indices which represent plant growth functions such as Leaf Area Index (LAI), Fractional Vegetation Cover, Biomass estimation, Photosynthetic Activity (APAR) and the measuring the chlorophyll content. Research is needed to better interpret canopy level reflectance, because of the multiple light interactions within the canopy (Kaufmann et al., 2010) due to complexity of the canopy structure. (Damm et al., 2011).

This main focus of this research is on the detection of forest stress using fluorescence measuring techniques through satellite imagery. This should give early indication of any possible changes in the forest functioning and health, around in Hong Kong's forested watersheds. Apart from anthropogenic factors, forest stress can be triggered by environmental factors such as soil salinity, drought conditions, and climatic change locally and globally. Preservation of Hong Kong's forests is also important as they serve as water catchments and forest helps in maintaining the quality of reservoir water. So protecting forest and implementing strategies for the reforestation activities or controlling those factors which are destroying the natural habitat is good for any country's national economy as well as for the environment as a whole. Studies have pointed out the problem

of contamination of the Dongjiang reservoir watershed in China, which supplies over 60 % of Hong Kong's freshwater due to surrounding economic activities. The basic aim of this research is to understand the emission of chlorophyll fluorescence for monitoring vegetation health, and to recommend the best SIF retrieval methodology for Hong Kong's vegetation, using space borne hyperspectral sensors.

1.4. Organization of this thesis

In the first chapter of thesis states the need to investigate the health of vegetated and forested areas in Hong Kong using SIF techniques from different platforms.

In Chapter 2 a detailed literature review presents the chronological development in understanding of Sun Induced Chlorophyll Fluorescence

Chapter 3 is an analysis of SIF methodologies discussed and used in this research for satellite-based and field-based measurements.

Chapter 4 deals with the relationship between Chlorophyll Fluorescence and vegetation indices. The SIF response to vegetation phenology and vegetation stress is compared to the response of different vegetation indices.

Chapter 5 presents and compares the results from the hyperspectral satellite sensor and field-based spectrometer.

Chapter 6 includes the discussion and conclusion derived from the overall results.

CHAPTER 2 LITERATURE REVIEW

Photosynthesis is the process through which plants make food. Plants absorb sunlight in the 400–700 nm wavelength range to make food for growth. This process of photosynthesis involves three steps. First the plant converts chemicals into carbohydrates to make food. Secondly, heat is released as a by-product. The third process is related to chlorophyll fluorescence in which plants release low energy photons during photosynthesis, which can give us information about the health of the plants.

When sunlight falls on the surface of a plant, high energy photons excite the electron into a higher orbit. It stays there for six nanoseconds before returning back to its lower energy state and, as a byproduct, releases a photon. This photon has lower energy than the photon that excites the electrons. This low energy photon is known as a fluorescence photon. Vegetation experts along with physicists devised several methodologies to detect it (Baker, 2008; Moya, 2004; Porcar-Castell et al., 2014). Because the signal is very weak, highly sensitive equipment were needed to detect it. Using different algorithms and methods, they were able to detect the SIF in the laboratory. Space-based Remote Sensing measurements of SIF are still in their infancy, mainly because there is no satellite working solely for the detection of Sun Induced Chlorophyll Fluorescence. There are several parameters we need to analysis for the measurement of chlorophyll fluorescence. The signal is coming from the satellite image and reaching the earth and then reflecting from the surface and reaching the satellite sensor. In between, the sunlight has to pass through the atmosphere. Atmospheric aerosol, water vapour and several particles may disturb the signal. The orientation of leaves and angle of the sun is important while calculating the

SIF. The spectral power of the sensor is also important for deciphering the weak signal of fluorescence, which is only 2.5 % of incident sunlight.

2.1. Remote Sensing of Vegetation physiology

Fluorescence-based studies are widely used for the large-scale monitoring of Gross Primary Productivity (GPP). GPP is the main vegetation productivity metric, representing the total amount of carbon fixed by vegetation due to photosynthesis. Remote Sensing Light Use Efficiency (LUE) models can be used to monitor GPP. The relationship of GPP with Photosynthetic Active Radiation (PAR) and the LUE fraction absorbed by vegetation (fPAR) for photosynthesis can be written as Eq 2.1 (Porcar-Castell et al., 2014).

$$GPP = PAR * fPAR * LUE \qquad \text{Eq 2.1}$$

The first two parameters can be derived by remote sensing. Vegetation indices are used to derive fAPAR and other coefficients such as the chlorophyll content and leaf area index (LAI). Using remote sensing, the LUE can be divided into plant functional types (PFT's). Then, combining PFT, vapor pressure deficit and temperature, LUE can be determined through remote sensing studies (Jeong et al., 2017). Because Chlorophyll-a fluorescence is linked with PAR, fPAR and LUE (Zhang et al., 2016), chlorophyll- a fluorescence retrieval studies, are important for accurate GPP estimates.

Using different vegetation indices, by exploiting the differences in surface reflectance between the red, blue, and near-infrared part of the spectrum, *f*APAR, green biomass, chlorophyll content, or leaf area index (LAI) can be calculated (Rouse et al., 1974).

Vegetation indices can provide good seasonal correlation with the GPP models in several plant communities such as grasslands, croplands and deciduous forests. For the evergreen forest, this correlation does not provide any suitable analysis, as seasonal changes in GPP are regulated by LUE and *f*APAR (Porcar-Castell et al., 2014).

In comparison with multispectral sensors, hyperspectral sensors provide narrow band characteristics suitable for detecting changes within the narrow spectral measurement which are useful ecosystem modelling (Kaufmann et al., 2010). This can retrieve subtle physiological responses from the vegetation and represent physical and chemical properties of the vegetated cover (Staenz et al., 2012).

To understand the physiological condition of vegetation, requires narrow bandwidths (5 nm or less), which are not measured by current satellite sensors (Wang et al, 2015). Narrow green wavelength bands can be used to directly calculate carbon flux using the photochemical reflectance index (PRI), $(\alpha_{531}-\alpha_{570})/(\alpha_{531}+\alpha_{570})$, where $\alpha_{531 \text{ and }} \alpha_{570}$ are the reflectances of very narrow bands with wavelengths 531 nm and 570 nm. Gamon et al., (1997) demonstrate that this index correlates highly with field measurements.

Red edge region of PAR

In the Photosynthetically Active Radiation (PAR) region of 660 - 800 nm, the reflected solar energy has a very small offset caused by fluorescence emission which amounts to 10 Wm^{-2} sr^{-1} u m^{-1} (Campbell et al., 2008)

This fluorescence which adds to the reflected wavelength can be monitored for the direct measurement of the photosynthetic activity of vegetation. A maxima of fluorescence can be found at 690 nm and 740 nm. The fluorescence signal causes a very minute reduction in the depth of absorption lines of O_2 and Fraunhofer lines, which is noticeable in the

saturated lines which are presented around the strong O_2A (765 nm) band, and the weaker O_2B band (685 nm).

Guanter et al., (2010) showed that introduction of a red edge band in the high spectral window of future satellites would be very beneficial for fluorescence studies. This short wavelength region between 720 nm and 740 nm also called the red edge region has a similar reflectance magnitude of fluorescence. The relative fluorescence signal is greater because of lower surface albedo within this region. (Zarco-Tejada et al., 2003) showed there is a good correlation between red edge region indices and radiance-based fluorescence using airborne spectrometer data.

2.2. Remote sensing of sun induced chlorophyll fluorescence

The first ever detection of fluorescence was by Joseph Fraunhofer (1817) who correctly identified dark lines in the continuous solar spectrum. He observed and provided insights that these dark lines were indeed of solar origin rather than terrestrial phenomena. These dark lines were first demonstrated by William Wollaston in 1833, but Fraunhofer suggested that these lines have a solar origin, thus they are called Fraunhofer lines. In 1833, Herschel further improved understanding that these lines were caused by both solar and terrestrial atmospheric absorption. The exact nature of these lines was further demonstrated by Kirchoff in 1861 while developing the method of modern spectroscopy (Ranjan S. Muttiah, 2002).

Table 2-1: Spatial scales of remote sensing platforms used for fluorescence retrieval in ecological studies.

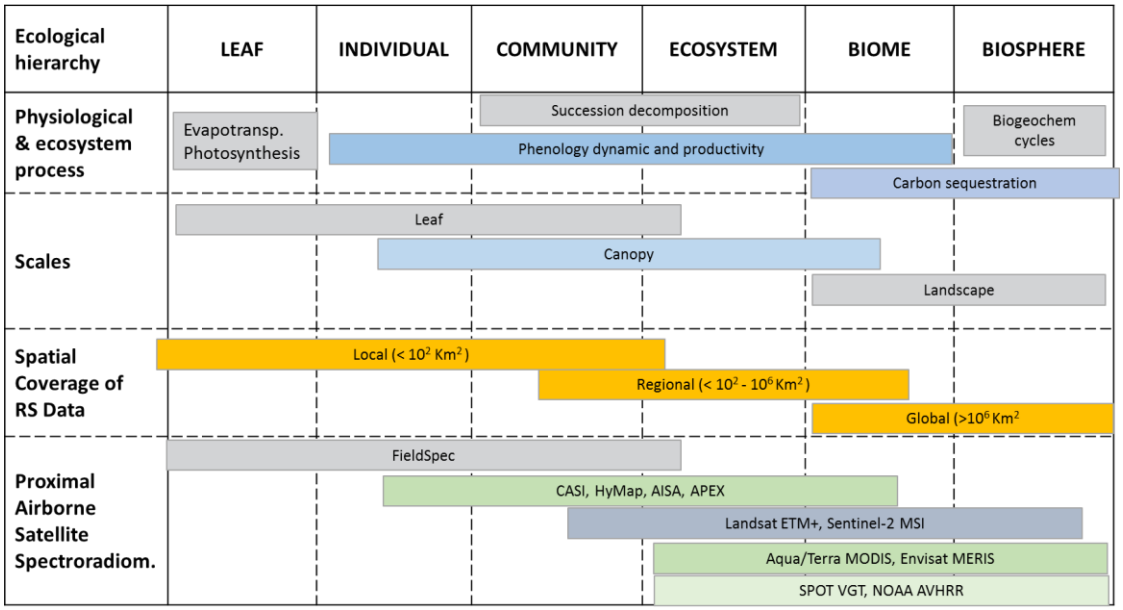

* inspired from (Homolová et al., 2013)

The chlorophyll content of plants has been estimated by measuring variations in the spectral bands in the visible and NIR region. The chlorophyll absorption region near 675 nm is useful to measure the amount of chlorophyll content in the plants. However, problems arise when medium to high chlorophyll content exists in plants, the sensor saturates and this index is not useful (Datt, 1998) Even the universally acknowledged NDVI has been found insensitive to medium to high chlorophyll concentrations (Zhang et al., 2014).

2.3. Sun induced chlorophyll fluorescence: mathematical basis

Solar energy when absorb by chlorophyll, is used in carbon fixation, heat dissipation and then is emitted at a longer wavelength in the form of chlorophyll fluorescence (Krause and Weis, 1991).

Radiance upwelling received by sensor consists of reflected solar flux and the fluorescence signal itself. Lambert's Cosine Law can be applied if we assume both reflected light and Fluorescence emission follows it. Considering Lambert's Cosine Law formula for radiance upwelling of the signal which consists of fluorescence and reflected flux eq one could be written as Eq 2.2:

$$L(\lambda) = \frac{\boldsymbol{r(\lambda)E(\lambda)}}{\boldsymbol{\pi}} + \boldsymbol{F(\lambda)} \qquad \text{Eq 2.2}$$

where λ is the wavelength of the upwelling and downwelling solar signal, r is reflectance, and E is the downwelling solar irradiance falling on the vegetation target. As discussed earlier, Fraunhofer first described the method to decouple this signal using FLD in 1975. Using this principle, radiance is measured within narrow dark lines in the solar irradiance spectrum. Measuring the intensity within those dark lines can be related to the reflected fluorescence. To exploit those dark lines in the solar spectra and two regions were found, in the oxygen absorption regions of the atmosphere, which can be used for retrieval of fluorescence. These regions are positioned at 687 nm and 760 nm respectively. The band depth which is the strength of these absorption bands, relies on the amount of oxygen present in the atmosphere and its interaction with the incoming sunlight. That is why it is very important to consider the water level information in the atmosphere and the atmospheric pressure of the region under investigation. During the day, band depth changes due to changes in solar elevation, as the relation between path length of light, and the cosine of solar zenith angle is inversely proportional. Using FLD, the amount of fluorescence can be estimated if we compare the wavelength of a measured radiance inside the dark line which can be represented by L (λ_{in}) and the outside of the dark line which is L(λ_{out})

By assuming both fluorescence and reflectance (r), constant FLD can be written as

$$L(\lambda_{in}) = \frac{\boldsymbol{rE}(\lambda_{in})}{\boldsymbol{\pi}} + \boldsymbol{F} \qquad \text{Eq 2.3}$$

$$L(\lambda_{out}) = \frac{\boldsymbol{rE}(\lambda_{out})}{\boldsymbol{\pi}} + \boldsymbol{F} \qquad \text{Eq 2.4}$$

Where L and E are upwelling radiance and downwelling radiance respectively, in and out of the absorption band. It should be noted that many authors have criticized the assumption of constant reflectance and fluorescence in this formula at distances away from the ongoing phenomenon.

Looking into the solar spectrum, the presence of narrow absorption lines can also be observed, which is due to atomic absorption in the sun's photosphere and chromosphere. These absorption lines which are very narrow are called Fraunhofer lines. These Fraunhofer lines are different from the O_2 absorption lines.

2.3.1. Retrieval of Fraunhofer lines

It has been shown and understood that isolated Fraunhofer lines are only affected by fluorescence, and that scattering does not have any major impact. For this reason, retrieval of Solar induced chlorophyll fluorescence is possible over these lines (Julitta et al., 2016). On a clear satellite image without haze or cloud, it is possible to retrieve fluorescence by using Fraunhofer line bands which have different physical properties from the O_2 absorption line bands. As there is little attenuation in the fluorescence signal within the Fraunhofer band, the signal reaching the sensor contains unbiased fluorescence information originating from the vegetated surface. By exploiting these bands retrieval of fluorescence is possible.

Damm et al. (2011) described a modeling study that isolates and quantifies the impacts of sensor characteristics, such as the spectral sampling interval (SSI), spectral resolution (SR), signal to noise ratio (SNR), and spectral shift (SS) based on the accuracy of SIF measurements in the oxygen A band centered at 760 nm (O_2A). In this study, SIF was retrieved using the three most common FLD retrieval methods, namely the original FLD method (sFLD) (Plascyk, 1975), the modified FLD (3FLD) (Maeir et al, 2003) and the improved FLD (iFLD) (Alonso et al., 2008). The analysis investigates parameter ranges, which are representative for field and airborne instruments currently used in SIF research (ASD FieldSpec, OceanOptics HR, AirFLEX, AISA, APEX, CASI, and MERIS). Frankenberg et al., 2011 further investigated the solar transmission spectrum, in order to analyse the depths and shapes of Fraunhofer absorption lines at full spectral resolution as well as the effect of fluorescence on O_2A band retrieval.

2.3.2. Fraunhofer lines retrieval windows

By exploiting the spectral region presented in the GOSAT and OCO_2, fluorescence has been successfully retrieved using the Fraunhofer lines bands. Two strong Fraunhofer line regions are mostly present. One is in the short wavelength region ie. the O_2A band at 757.5 nm. This region does not contain any telluric lines and the maximum transmission is 44% at 758.51 nm at full spectral resolution. This region also contains four strong Fraunhofer lines.

The second region is between 769.5 and 775 nm, overlapping weak O_2 lines. It is at the very strong potassium (K) Fraunhofer lines region at 770.1 nm. In this region, transmission is below 20 % at full spectral resolution. As discussed earlier, scattering is stronger at the lower frequency, and this region overlaps the O_2 band, hence radiative

transfer modelling is preferable to avoid any biases in the retrieved results due to the presence of O_2 lines and their interference in the fluorescence signal. Joiner et al (2010) use this window to exploit the fluorescence signal using GOSAT satellite. To minimize the effect of O_2 lines in these regions, the IMAP-DOAS approach can be applied, as demonstrated by Frankenberg et al (2005).

2.3.3. Fluorescence spectral bands

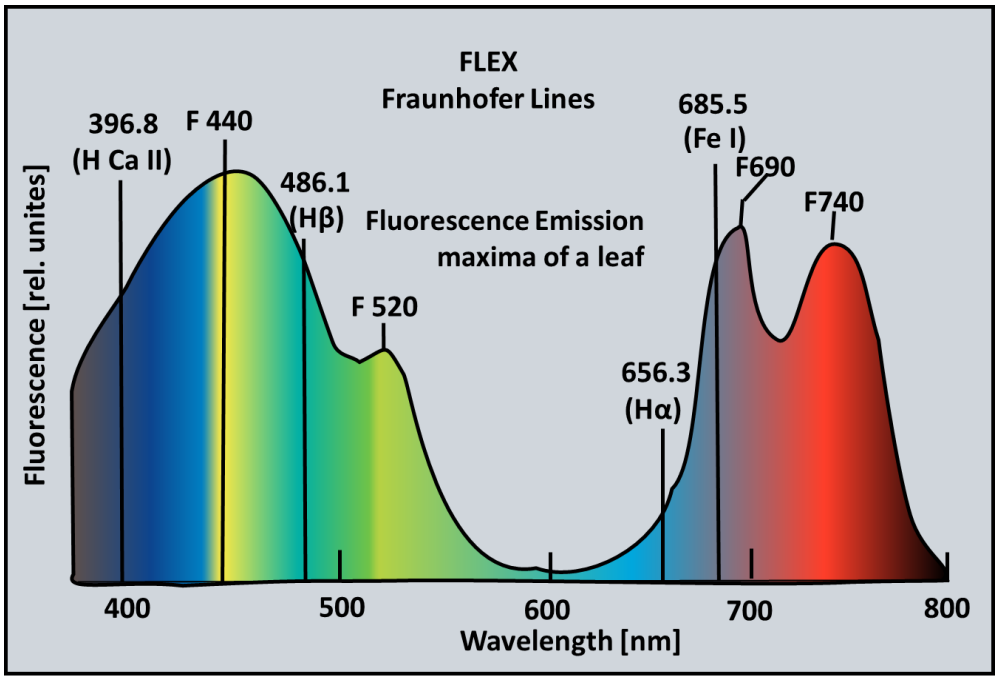

Figure 2-1: Fluorescence emission under natural sunlight
Source: (Davidson et al., 2003)

Healthy green vegetation emits a chlorophyll fluorescence signal maxima around 440 and 520nm and in the red and far-red around 690 and 740 nm respectively as shown in the Figure 2-1 (Davidson et al., 2003). The blue-green band emittance of fluorescence is due to the epidermis of the plant which can provide additional information about the plant status. The red and far-red chlorophyll fluorescence are due to the mesophyll which is a

highly photosynthetically active part of the leaf tissue. Literature recommends the red and far-red fluorescence bands for vegetation health monitoring by fluorescence (Moreno et al., 2006), as the signal is much stronger. Indeed, the Fraunhofer lines or oxygen absorption lines combined provide the main fluorescence bands andO_2A and O_2B bands are considered mandatory for the measurement of SIF.

2.3.4. The range of fluorescence values

Several studies demonstrate that the O_2A oxygen absorption band SIF values range from 0 to 17 W m^{-2} sr^{-1} μm^{-1} and at O_2-B oxygen absorption band around 685 nm its value ranges from 0 to 36 W m^{-2} sr^{-1} μm^{-1}. These ranges depend on several factors including vegetation species type, the level of investigation such as leaf level or canopy level, canopy structure, phenology, illumination, and stress factors (Michele Meroni et al., 2009). The range of fluorescence for both bands includes the maximum and minimum values under different circumstances. In Table 2-2 different fluorescence values have been presented as found in different studies (Raychaudhuri, 2014b).

Table 2-2: Range of SIF retrieved through different sources

Literature	Oxygen Absorption Band	Result Range of SIF	Description
Meroni et al. (2009)	O_2A	0 - 20	Review of field based, air-borne and space-based SIF studies
	O_2B	0 - 36	
Guanter et al. (2007)	O_2A	0.6	CASI (Airborne) and MERIS (Space Based)
Zarco Tejada et al. (2009)	O_2A	0 - 0.38 (Healthy)	Aerial platform sensor-based results
		0 - 2.2 (Stressed)	
Guanter et al. (2010)	O_2A	0 - 3	Field Based results
	O_2B	0 - 2	
Joiner et al. (2011)		3	GOSAT Simulated Result
Frankenberg et al. (2011)		2.50%	Simulation Continuum Spectrum of 2.5%
Guanter et al. (2012)		0 -1.8	Global retrieval of SIF
Joiner et al. (2013)		0 - 6	Simulated Results
Barun Raychaudhuri (2014)	O_2A	0 - 1.87	Hyperion Based SIF retrieval

Source: (Raychaudhuri, 2014b)

Healthy vegetative canopies have been found to have a fluorescence peak value at O_2A band around 2 mW/m^2 /sr/nm. Grasslands are found to have higher fluorescence emission than needle-leaf forest and crops: around 1.5 5 mW/m^2 /sr/nm at 760nm (ESA-HYFLEX, 2013)

Rossini et al., (2014) showed maximum fluorescence emissions found in crops compared to broadleaf and needle-leaf species, with needle leaf having the lowest fluorescence values.

2.4. Factors affecting fluorescence retrieval

Factors which affect the fluorescence radiance at 761 nm include sun zenith angle (θ), fluorescence quantum efficiency (Fi), leaf inclination distribution function (LIDF), leaf temperature (T), leaf area index, and leaf chlorophyll a + b content (chl-a+b) (Ni et al., 2015). The sensor specification also plays a large role in accurate retrieval of SIF. The spectral sampling interval (SSI), Spectral Shift of the spectral range (SS), Signal to Noise Ratio (SNR) of the sensor, and the Spectral Resolution (SR) are considered to be the most important sensor-related factors and in deciphering the SIF signal from the upward flux received by sensor (Damm et al., 2010). It has been proved experimentally that the temperature affects the emission of the fluorescence signal. Hence thermal images from the satellite sensor may provide another insight about the plant dynamics such as transpiration and stomata closure which ultimately leads us towards the better detection of fluorescence emitted signal (Meroni & Colombo, 2006).

Non-photochemical quenching plays a significant role in inducing chlorophyll fluorescence emittance. Hence steady-state chlorophyll fluorescence is highest in the early morning up to 10 am, then decreases until early afternoon reaching its minimum and then possibly recovering slightly by evening. Eco physiological research suggests that the best possible fluorescence signal is around 8 to 9 am, but to gather the full solar illumination and fluorescence signal both satellite sensor and ground-based observations should be made around 10 am local solar time (Moreno et al., 2006).

2.4.1. Aerosol and atmospheric effects

Research indicates that remotely sensed fluorescence retrieval in both O_2A and O_2B regions can have bias due to instrumentation and environmental parameters. These include errors in aerosol optical depth (AOD) retrieval, aerosol model and vertical profile, surface pressure, polarization, temperature profiles or radiometric or spectral errors. Figure 2-2 shows the placement of atmospheric absorption bands with respect to the vegetation spectral response.

By using the least squares retrieval method for fluorescence, (Frankenberg et al., 2011) showed that Fraunhofer lines around the O_2A band can be used for estimation of aerosols presence in the atmosphere, and provide better results because the effect of fluorescence due to atmospheric scattering is considered in the calculation. For aerosol estimation, if the effect of fluorescence is not included, results can be biased.

Raman scattering has been shown to have a negligible effect at low solar zenith angles and high surface albedo, and that is the main reason rotational Raman scattering can be ignored during the calculation of radiances from the radiative transfer model (Chance and Spurr, 1997)

Inelastic scattering can also be ignored in the models but places where fluorescence is minimal such as non-vegetated surfaces, inelastic scattering should be considered for the better understanding of the impact of fluorescence on the O_2A band (Montagna, 2008)

Fluorescence signal retrieval problem. The most serious problem that may occur for fluorescence retreival is that even after the retrieval of SIF one cannot be sure of its input in the overall energy balance because there is a third process that takes place during the process of photosynthesis which has a significant role, namely heat dissipation: and in the case of photo inhibition it has more emphasis in the overall balance. Consequently we

cannot be sure how much fluorescence is related to the overall photosynthesis process until we also calculate heat dissipation (Meroni et al., 2010).

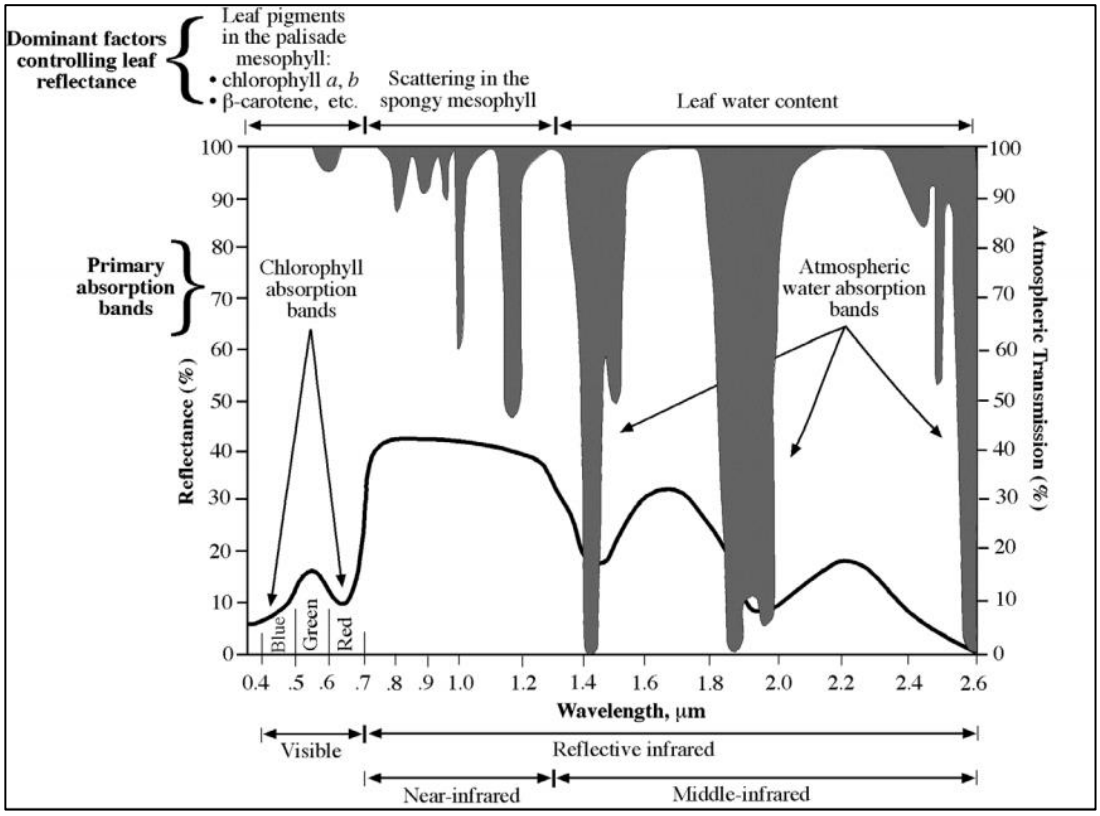

Figure 2-2: Vegetation spectra and absorption in the atmosphere

Source: (Jensen, 2007)

2.4.2. Error arising due to low SNR and FWHM narrow band selection

The signal to Noise Ratio (SNR) is the most important sensor parameter for retrieval of accurate SIF. With high SNR, better precision can be achieved even with lower spectral resolution. As shown by (Frankenberg et al., 2011) using OCO-2 data and GOSAT data, higher SNR of OCO-2 gave better precision compared to GOSAT. (Damm et al. (2010) also showed that strong SNR compensates the low spectral resolution, finding that SR accounts for 40 % of the overall retrieval error.

2.5. Guidelines for fluorescence retrieval

Meroni et al.(2009) mentioned the following guidelines for accurate fluorescence retrieval from space platforms:

(1) Understanding the light that is effectively absorbed by chlorophyll and the total light absorbed by the plant

(2) Validating the fluorescence retrieval through Fraunhofer and O2 line in-filling methods

(3) Application of basic vegetation indices for making an accurate relationship between vegetation variables and the fluorescence signal.

(4) Identification of different plant species and devising the methodology for the retrieval of fluorescence for each plant type.

(5) Performing accurate atmospheric correction understanding the spectral illumination source and its relationship with the vegetated cover .

(6) Selection of suitable bands and the sites which must be cloud free during the time of satellite image acquisition.

Downwelling irradiance plays an important role in remote sensing-based studies or vegetation. It has been shown that irradiance values can vary index calculations such NDVI (9%) and PRI (12%) (Damm et al., 2015). If exact irradiance measurements and anisotropic reflectance information are not included in the calculations then uncertainties in the ranges have been found to be 13 % for NDVI, 32 % for PRI and 58 % for SIF .

CHAPTER 3 FLUORESCENCE RETRIEVAL METHODS

Solar-Induced Chlorophyll Fluorescence detection methods are recognized by the scientific community as belonging to two types: radiance-based and reflectance based methods (Meroni et al., 2009). Additionally, scientific methodologies for the understanding of SIF are different for different platform. Figure 3.1 shows the main processes of SIF retrieval using both active and passive remote sensing methods.

3.1. Active methods

There are two main methodologies for the measurement of Chlorophyll fluorescence. In the active methodology artificial light is use to excite the leaf for fluorescence measurement. Active methods are based on PAM (Pulse Amplitude Modulation) systems and Laser Remote Sensing technology at the laboratory level (Kolber et al., 2005) has been developed and tested for SIF retrieval but their applicability at the canopy and landscape level is still not fully understood (Wolanin et al., 2015). These methods describe the relative perturbations in the Chlorophyll fluorescence mostly in the light adapted plants. Using active methods several other fluorescence measurements can be determined such as minimal fluorescence (in the absence of sunlight) and maximum fluorescence (emitted after bombarded with the laser which consists of the specific light pulse to induce the chlorophyll fluorescence). Range of active methods for the measurement of fluorescence is limited from centimeters to meters. (Candrero-Mateo MP et al., 2016).

3.1.1. Laser-based methodology

Extensive laboratory studies of plant photosynthesis have been carried out using active excitation techniques such as laser-induced chlorophyll fluorescence with the use of modulated light and saturating pulses. These techniques have not been explored through space base platforms as they have some technical issues

3.1.2. Pulse amplitude modulation (PAM)

In vivo understanding of fluorescence is based on Pulse Amplitude Modulated (PAM). In PAM fluorimeters pulse modulation technique is used and it is able to measure fluorescent kinetic curve of plant. It is designed by Dr Ulrich Schrieber (WALZ Coporation). PAM fluorometry is a laboratory-based method for SIF measurement across a wide spectral region, hereas SIF methodology uses very narrow spectral regions. The other difference between SIF and PAM is that PAM is not affected by ambient illumination whereas for the measurement of SIF, great care should be taken for the detection of fluorescence signals as they are greatly affected by atmospheric conditions.

3.2. Passive Methods

Passive methods have been used to measure fluorescence from plants both on leaf and canopy scales (Candrero-Mateo MP et al., 2016). Both active and passive methods are used to measure chlorophyll fluorescence diurnal and seasonal basis. Passive methods do not rely on the artificial light. In fact, solar irradiance and consequently radiation emitted by the plants is used for the quantification of SIF. In passive methods, solar irradiance absorption bands are used which is termed as Sun Induced Chlorophyll Fluorescence SIF. Most common methodology that is applied to decipher the chlorophyll fluorescence is

Fraunhofer Line Discriminator method (FLD) (Plascyk., 1975). (This will be explained in detail in the later sections).

Photosystem 1 (PSI) and photosystem 2 (PSII) are the pigments in the plants that collect energy from the sunlight over the broad range to generate an electron to the higher level and then drops to the lower level after sometime in the process it releases energy to pass on to the next pigment. Each system works together by using sun energy to create energy for the plant. PSI consist of Chlorophyll a molecule and it absorbs energy at maximum 700 nm. PSII consist both Chlorophyll a and Chlorophyll b. PSII absorbs light at 680 nm (Frankenberg et al., 2014).

Table 3-1: SIF retrieval with active and passive methods

	Active methods	**Passive Methods**	
Methodology	PAM (Licor 6400)	FLD (iFLD,3FLD)	Filtered illumination (Fluowat)
Measuring Light	Artificial Modulated	Sunlight	Sunlight or Filtered Artificial
Wavelength Range	700 to 715 nm	687 nm (O2B Band)	Complete Spectrum of SIF
		763 nm (O2A Band)	
Main Contributors	PSII & PSI	PSII & PSI	PSII & PSI
Distance	Field based and Airborne (cm to m)	Field based, airborne and Space	SIF emission spectrum limited to the area without light
Measurement type	Relative fluorescence yield	Emission radiance of SIF at absorption bands	Emission spectrum of of SIF in radiance

Source: (Amoros-Lopez et al., 2008)

3.2.1. Radiance based methodology

The fluorescence signal is very weak compared to other emitted signals and detecting it from space is challenging, as it is only a small fraction, i.e., 0.5–2% of reflected solar

radiation emitted from the surface (Frankenberg et al. 2012). The SIF spectrum is able to disentangle the reflected radiance and SIF emissions by comparing the radiance inside and outside the oxygen absorption bands. Below are some of the extensive used Radiance based methods for the retrieval of SIF.

3.2.1.1. Fluorescence retrieval based on the FLD method

The Fraunhofer Line Discriminator FLD principle is based on spectral radiance, and was first described by Plascyk (1975). It uses sun irradiance and canopy radiance inside the Fraunhofer line and outside to detect the SIF. It has some disadvantages such as reflectance and fluorescence of the inside bands, and the outside bands are considered the same. By Inside and outside the reflectance bands it means for the measurement of fluorescence at 680 nm one wavelength below 680 nm is selected (Example 670 nm) and one wavelength outside (Example 690 nm) is selected to decipher the SIF by using mathematical formulas such as FLD. Several researchers played their role to further improve these methodologies by implementing the new methods improved FLD (Rascher et al., 2015) extended FLD (Mazzoni et al., 2010) especially the spectral fitting methods (Panigada et al., 2010).

In FLD methods, SIF is calculated in radiance unit by considering the Sun irradiance (J. Plascyk, 1975) as shown in Eq 3.1.

$$\mathbf{SIF} = \frac{\mathbf{E_{out}\, L_{in} - L_{out}\, E_{in}}}{\mathbf{E_{out} - E_{in}}} \qquad 3.1$$

Whereas E refers to the wavelength in irradiance spectrum and L refers to the radiance wavelength. Out and in subscripts refers to the bands outside and inside of wavelength at which fluorescence value needed to be retrieved. Four values need to be known to retrieved fluorescence from the FLD method, Two irradiance wavelengths inside and

outside of particular wavelength and Two radiance wavelengths inside and outside of the fluorescence wavelength for centre wavelength.

3.2.1.2. The sFLD method

Plascyk (1975) presented the sFLD method, in which one band is used as a reference band, and the other band is the fluorescence band at 760.6 nm. The ratio of both these bands gives fluorescence (Fs) as: Eq 3.2

$$Fs = \frac{L1 - \frac{E_1^0}{E_2^0} \cdot L_2}{1 - \frac{E_1^0}{E_2^0}} \qquad 3.2$$

Where E^0 represent the irradiance and L represents the canopy radiance, 1 represents the fluorescence band at O_2A absorption band and 2 represent the reference band.

3.2.1.3. The iFLD method

(Alonso et al., 2008) showed that assuming a relationship between fluorescence and upward Flux R within the observed wavelength, will produce inaccuracies in the fluorescence values. Their new improved FLD (iFLD) method using non-linear variations in both R and Fs, shows that results can be improved. This method falls into the category of non-linear differential absorption techniques (Damm et al., 2010). In the iFLD method correction is done by applying non-linear interpolation to the apparent reflectance. Fluorescence impurity is denoted by aF, and pure reflectance which does not have any fluorescence signal is denoted by the aR nearby absorption band. In this method, interpolated reflectance from a vegetated surface is denoted by iRL and interpolated reflectance from non-vegetated surface is denoted by iRE^o. The fluorescence formula can be written as Eq 3.3

$$F_S = \frac{L_1 \cdot aR - \frac{E_1^0}{E_2^0} \cdot L_2}{aR - \frac{E_1^0 \cdot aF}{E_2^0}} \quad 3.3$$

Where as $\boldsymbol{aR} = \frac{iRL_2}{iRL_1}$ and $\boldsymbol{aR} = \frac{iRE_2}{iRE_1}$

In iFLD, the most important consideration is the selection of the absorption band and reference band radiances. Overall results of iFLD have shown to be much better than the original FLD method.

3.2.1.4. The 3FLD Method

The 3-FLD method (Maeir et al. 2003) can be used to retrieve fluorescence in the O_2A band.

It is proven that the original FLD method largely overestimates the fluorescence signal whereas the improved FLD method (iFLD) and 3FLD provides more accurate estimates of the Fluorescence value (Damm et al., 2010)

3.2.2. The Damm method

In the Damm method O_2A oxygen absorption band along with 3FLD method used to retrieve SIF. TOA radiation can be simulated along with the fluorescence by using atmospheric correction models such as MODTRAN 4 and SCOPE. Retrieval of fluorescence from these models usually assumes that SIF and reflectance always follow lamberts law. By considering this assumption, TOA radiation which contains the SIF can be written as Eq 3.4 (Damm et al, 2010).

$$\mathbf{L_{TOA}} = \frac{E_{0cos\theta}}{\pi}\boldsymbol{\rho_{so}} + \frac{E_{0cos\theta}}{\pi}\frac{(\tau_{ss}+\tau_{sd})\,R(\tau_{do}+\tau_{oo})}{1-R\rho} + \frac{SIF(\tau_{do}+\tau_{oo})}{1-R\rho} \qquad 3.4$$

L_{TOA} is the TOA radiation signal. The first ratio after the equal sign is the surface reflectance regarding radiance. The last ratio includes information about SIF. Whereas terms in the equation contain ρ_{so} is hemispherical reflectance (it is the reflectance from a surface that is under direct illumination), Θ is the solar zenith angle, R is the surface reflectance, SIF is for the Top of the Canopy (TOC) ρ is the spherical reflectance from the atmosphere to the surface. T is Transmittance, ss in the subscript represents incident radiation, and oo represents scattered radiation.

The Damm method assumes negligible atmospheric scattering and absorption on the canopy scale. By applying this assumption, Equation 3.5 can be written in the simplified form as Eq 3.5 below

$$\boldsymbol{L} = \frac{E_g R}{\pi} + \boldsymbol{SIF} \qquad 3.5$$

Where E_g Corresponds to $E_0\cos\Theta$. According to the 3FLD principle the SIF formula can be written as Eq 3.6

$$SIF_i = \frac{L_i - \frac{E_g^i \times (\omega_{left} \times L_{left} + \omega_{right} \times L_{right})}{\omega_{left} \times E_g^{left} + \omega_{right} \times E_g^{right}}}{1 - \frac{E_g^i}{\omega_{left} \times E_g^{left} + \omega_{right} \times E_g^{right}}} \qquad 3.6$$

$$\omega_{left} = \frac{760 - 753}{771 - 753}, \ \omega_{right} = \frac{771 - 760}{771 - 753}$$

Where i indicates the 753 nm band which is inside the fluorescence peak band at 760 nm, and o represents the band 771 nm.

The above equation corrects for atmospheric scattering and absorption during field data collection. By assuming fluorescence and reflectance shows linear variation both inside and outside of the absorption band O_2A final SIF equation can be written as Eq 3.7

$$SIF_i = B\left[\frac{X_i\,(E_g^0 + \prod X_0 \rho_0) - A X_0 (E_g^i + \prod X_i \rho_i)}{B(E_g^0 + \prod X_0 \rho_0) - A(E_g^i + \prod X_i \rho_i)}\right] \qquad 3.7$$

where $X_j = \frac{L_j - L_p^j}{\tau_j \uparrow}$ and $E_g^j = \frac{E_0^i \cos\theta}{\pi}(\tau_{ss}^j + \tau_{sd}^j)$

J = i, o, B – SIF_i/SIF_o. i and o represent the bands inside and outside the O_2A absorption bands and have value equal to 0.8 (Alonso et al., 2008).

Whereas $A = \frac{\rho_{758}\omega_1 + \rho_{771}\omega_2}{\rho_{758}}$, $\omega_1 = \frac{771-760}{771-758}$, $\omega_2 = \frac{760-758}{771-758}$

Whereas Ni et al (2016) retrieved SIF using DOAS and Damm method and conclude that these two methods have the strongest correlation with SIF retrieval from the SCOPE model; they concluded that the Damm method has the best performance in the O_2A Oxygen absorption band for their requirement.

3.2.3. The Barun method

The Barun methodology has been used in this research for the detection of SIF using Hyperion satellite sensor by applying the Fraunhofer Line Depth method (Plascyk, 1975) in the O_2- A band. This has been used in many previous studies for the retrieval of the

chlorophyll fluorescence signal from space-based measurements. Raychaudhuri (2014a) proposed a new fluorescence retrieval method from hyperspectral images and validated his findings with laboratory-based experiment. He proposed a methodology to compare the radiation ratio of O_2A band and bands inside and outside the O_2A bands from vegetated and non-vegetated surfaces respectively. Hence the effect on both surfaces will be the same. After this assumption, he assumed the fluorescence wavelength reaching the sensor is a linear combination of incident radiance reflected from the object so the difference at sensor can be written as Eq 3.8.

$$D = \omega_L L_L + \omega_R L_R - L_F \qquad 3.8$$

The quantity D, which is the difference at the sensor from both vegetated and non-vegetated surfaces and has a unit of radiance (Wm^2sr^{-1} u m^{-1}) L_F is the O_2A radiance wavelength, whereas L_R and L_L represent the radiance wavelengths to right and left of the O_2A band respectively. So the relative wavelengths $\omega_L$and ω_R concerning wavelength at left and right of the O_2A wavelength can be written as follows

$$\boldsymbol{\omega_L = \frac{\lambda_R - \lambda_F}{\lambda_R - \lambda_L}}$$

and

$$\boldsymbol{\omega_R = \frac{\lambda_F - \lambda_L}{\lambda_R - \lambda_L}}$$

He introduced the constant A, which is experimentally deductable and can be applied because all surfaces have limited reflectance at the particular wavelength. So the above equation can be written after dividing the Eq 3.9 by $\omega_L L_L + \omega_R L_R$

Therefore, another quantity (A) is

$$\mathbf{A} = \frac{\mathbf{D}}{\omega_L L_L + \omega_R L_L} = \mathbf{1} - \frac{L_F}{\omega_L L_L + \omega_R L_R} \qquad 3.9$$

He assumed for the case of Hyperion values of ω_L and ω_R as 0.5 because if there is no absorption at the fluorescence wavelength at sensor, then A will be equal to 0 whereas if there is total absorption, then A will be equal to 1. By putting 0.5 in the above equation we get the following equation Eq 3.10:

$$\mathbf{A} = \mathbf{1} - \frac{L_F}{0.5\,(L_L + L_R)} \qquad 3.10$$

By calculating A for both vegetated surfaces and non-vegetated surfaces, all the atmospheric parameters can be neglected because, at sensor, if vegetated and non-vegetated target are close enough, all the atmospheric effects will cancel out each other. Also, the path radiance will be equal in both cases (Raychaudhuri, 2014b)**.** The final Fluorescence formula using the Barun method is shown in the Eq 3.11 below

$$F = AV - ANV \qquad 3.11$$

A_V is the absorption from the vegetated surface and A_{NV} is the absorption from the non-vegetated surface. Modification of Barun method namely FLD-M has been used in this study. Detail of the extension can be found in Methodology Chapter.

3.2.4. DOAS

Platt (2017) introduced the Differential Optical Absorption Spectroscopy (DOAS) method, which deals with atmospheric trace gas concentration in the atmosphere for the retrieval of fluorescence. By calculating the absorption characteristics of trace gas molecules in the atmosphere, quantitative retrieval of fluorescence is possible. For this method, relative transmitted light intensity needs to be measured over a very broad spectral interval. Secondly, a high pass filter must be used to eliminate the effect of

Rayleigh and Mie scattering to obtain a differential absorption signal. Lastly, trace column densities must be quantitatively determined by comparing the observed spectra with the reference spectra by using least square methods. This method is based on Beer-Lambert Law. The DOAS fluorescence retrieval method can be expressed as Eq 3.12.

$$-\ln\frac{L(\lambda,\theta)}{E_g(\lambda,\theta)} = \sum_{n=1}^{n}\sigma_n'(\lambda)S_n + \sigma_{Ray}(\lambda)S_{Ray} + \sigma_{Mie}(\lambda)S_{Mie} + \sigma_f(\lambda)S_f + \sum_{m=1}^{M}a_m\lambda_m \quad 3.12$$

In which L(lambda) and E_g(lambda) is the backscattered radiance and solar irradiance respectively, Sn is the Aerosols particles in the atmospheric path, σ_n (λ) is nth atmospheric absorber, Rayleigh Scattering and Mie Scattering and fluorescence represented by $\sigma_{Ray}(\lambda)$, $\sigma_{Mie}(\lambda)$ **and** $\sigma_f(\lambda)$ respectively. $\sum_{m=1}^{M}a_m\lambda_m$ is the low order polynomial.

DOAS Eq 3.12 can be simplified according to (Khosravi, 2012) can be written as Eq 3.13

$$-ln\frac{I(\lambda,\theta)}{I_0(\lambda,\theta)} = \sigma_f(\lambda)S_f + \sum_{m=1}^{M}a_m\lambda_m \quad 3.13$$

In this equation M is set to 3. (Ni et al., 2016) investigated this method using field-based spectrometry data and observed a good correlation with the SCOPE model, concluding that DOAS has equally good accuracy. The only parameter that may effect the retrieved value using this method is the vertical distribution of the aerosol concentration (VIS) deduced from the model MODTRAN. VIS can be written as a function of AOD at 550 nm. For the O_2A band VIS is very sensitive and has a large impact. They observed that due to changes in the VIS , in the DOAS method has around 61.8 % of the fluorescence variations. For the DOAS method SZA, sensor height and elevation can be neglected.

3.2.5. Spectral fitting method

The Spectral Fitting Method (SFM) (Meroni et al., 2010) assumes that radiance and fluorescence within the selected spectral range can be explained using a different mathematical function such as polynomials. Upwelling radiance can be written as Eq 3.13 below, by considering these factors in the FLD method

$$\boldsymbol{L(\lambda)} = \frac{\boldsymbol{r_{MOD}}\,\boldsymbol{(\lambda)E(\lambda)}}{\boldsymbol{\pi}} + \boldsymbol{F_{MOD}(\lambda)} + \varepsilon(\boldsymbol{\lambda}) = \boldsymbol{L_{MOD}(\lambda)} + \varepsilon(\boldsymbol{\lambda})$$

$$\lambda \in [\boldsymbol{\lambda_1}, \boldsymbol{\lambda_2}] \qquad 3.13$$

Where MOD represents the modelled radiance and fluorescence and ε(λ) represents the difference between these two coefficients (Meroni et al., 2010)

The second spectral fitting method (SFM-2) was also developed using radiance data and different spectral windows, with the main focus on the Oxygen absorption bands. This second method is widely used for TOC spectrometer studies. The first ever maps from using this method at the 760 nm window, are now available. These results proved vital for aerial based studies and helped to develop the algorithm for the forthcoming FLEX platform by ESA (ESA-HYFLEX, 2013).

3.2.6. Statistical approach to retrieve SIF

The FLD and SFM methods both require the simultaneous acquisition of irradiance data. Using white reference and cosine receptors sometimes proves inaccurate for time series measurements because of atmospheric contamination. As alternatives, statistical approaches to FLD and SFM-based methods have proved successful for retrieval of SIF. The statistical methods involve low-frequency, and high-frequency components, which combine to form the fluorescent spectra. High-frequency components can be retrieved by

training of non-fluorescent spectra by principal components. The low frequency components are then derived from mathematical functions. Solar irradiance measurement is a necessity for both FLD and SFM methods because both require upwelling and downwelling radiance.

3.3. Reflectance-based methodology

In the reflectance base methodsthe set of two or three spectral reflectance's, and the wavelength that is effected by the fluorescence between 685 to 740 nm is used to create different vegetation indices related with fluorescence from vegeation. In this method fluorescence has no phsyical unit and it is measured qualitatively. (Tol et al., 2014) To perform this, several methods have been proposed such has reflectance indices (Zarco-tejada et al., 2000) derivative ratios (Zarco-Tejada et al., 2003) in filling method (Ni et al., 2015)

These reflectance-based methods present a quick way to monitor the fluorescence signal emitted by the vegetation cover because only two or three bands are required for developing the different indices.

Table 3-2: Fluorescence Retrieval Methods

Fluorescence Retrieval Methods	Methodology	Developed (Year)	Detail
Fraunhofer Line Discrimination (FLD)	Radiance Based	1975 (J. A. Plascyk, 1975)	This method by ignoring atmospheric effect can differentiate between fluorescence and non-fluorescence objects. But this method performs weaker in broad absorption bands.

Spectral Fitting Method	Radiance Based	2006 (Meroni and Colombo, 2006)	This method uses spectral curve fitting method to retrieve reflectance and fluorescence. Also it utilizes atmospheric radiation transfer modeling. Mainly focused on two oxygen absorption bands. Disadvantage of this method is that to use this method very high spectral resolution with Full width Half Maximum (FWHM = 0.1 nm) has to be utilized. This method is really complex and high computational time is required.
3FLD Method	Radiance based	2003 (Maier et al., 2003)	In this method reference band λout is replaced by two bands average of absorption line which solves the limitation of FLD method. But this assumption creates the invalidity of linearity of reflectance and fluorescence. Also, this method gives poor estimates for O_2B band.
iFLD Method	Radiance Based	2007 (Alonso et al., 2008)	This method finely removes the effects by atmosphere. Also removes the bias in fluorescence estimates. . This method uses the interpolation method and highly sensitive to this method.
Reflectance Ratio	Reflectance based (Perez-Priego et al., 2015)		Utilizes the range between 650 nm to 800 nm. Uses the red edge region. Without any complex math. Based on the assumption that one band must be affected by fluorescence while other should not be disturbed by fluorescence emission. This method is more susceptible to plant chlorophyll content.

CHAPTER 4 DATA USED AND METHODOLOGY

4.1. Study area

Hong Kong is a special administrative region of the Peoples Republic of China. It lies below the Tropic of Cancer on the southeast coast of China, and at the mouth of Pearl River Delta. The geographic centre of Hong Kong is 22, 15 N, 114, 10 E. Four main regions of Hong Kong are The Kowloon Peninsula, Lantau Island, Hong Kong Island and the New Territories, along with 262 small outlying islands. Hong Kong has more than 7 million population (Census and Statistics Department, 2016) which resides within 25% of the land due to steep terrain, and a total area of 1104 km^2. Due partly to the steep terrain, about 40% of Hong Kong area is Country Parks and nature reserves. Hong Kong lies in the subtropical climatic zone, having a mean annual temperature of 23 ^oC, with a cool and dry winter and a hot and humid summer. The annual rainfall is around 1924.7 mm (Hong Kong Observatory, 2017).

The study area spans an area of ~2800 ha comprising the Tai Mo Shan and Shing Mun Country Parks in New Territories, Hong Kong (Figure 4-1). The topography of the area in rugged characterized with convex slopes rising to the tallest mountain (957 m) of Hong Kong at Tai Mo Shan, and steep-sided slopes around Shing Mun reservoir. Upper valleys are covered with grasses - mostly fire-maintained grasses, and lower elevations are covered with patches of secondary forest and plantations (Delang and Hang, 2010). Temperature falls below zero, above 400 m elevation, several times in a decade and rainfall increases with elevation.

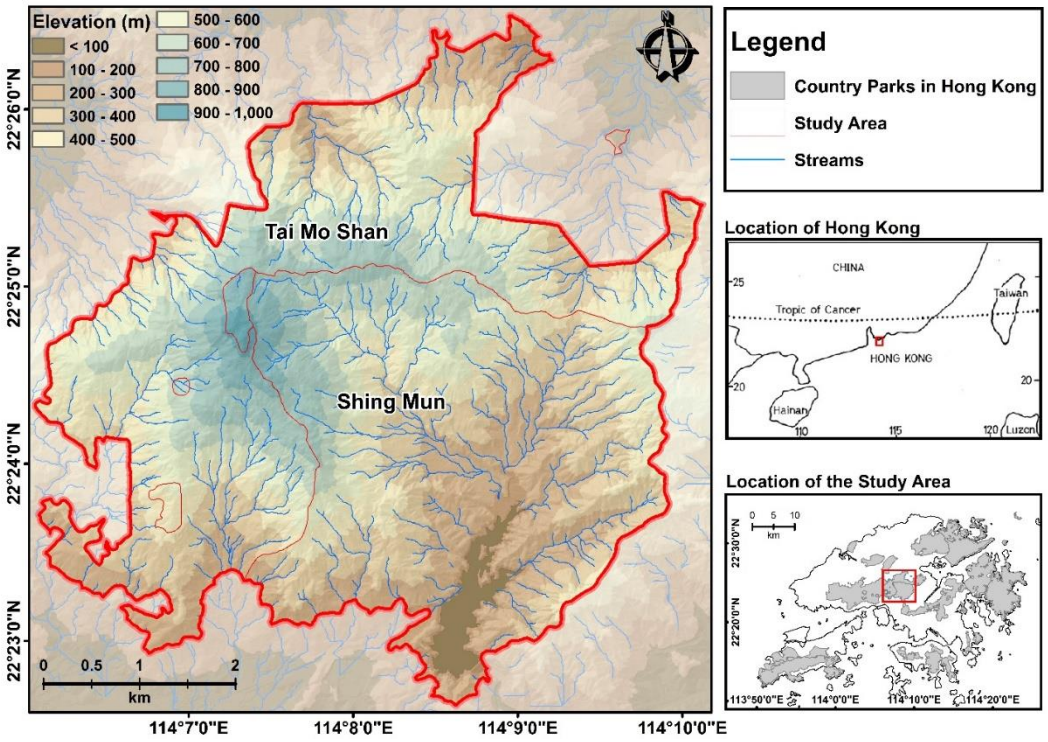

Figure 4-1: Location and topography of the study area

4.2. Structural vegetation types in study area

The structural vegetation types along with different age of forest species in the study area are shown in Figure 4-2 and Figure 4-3 respectively (Abbas et al, 2016). Grassland is one of the three major types of vegetation that can be defined as graminoid plants according to the International Biological Program. Shrubland is a plant community dominated by shrubs, often including grasses, herbs and geophytes, and forest is a large area covered mainly with trees and undergrowth.

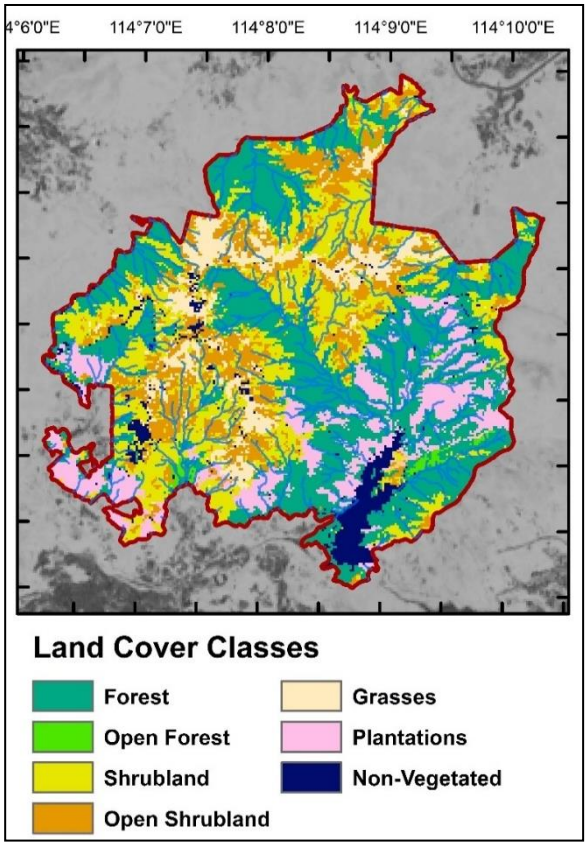

Figure 4-2: Habitat map indicating dominant vegetation cover types in the study area

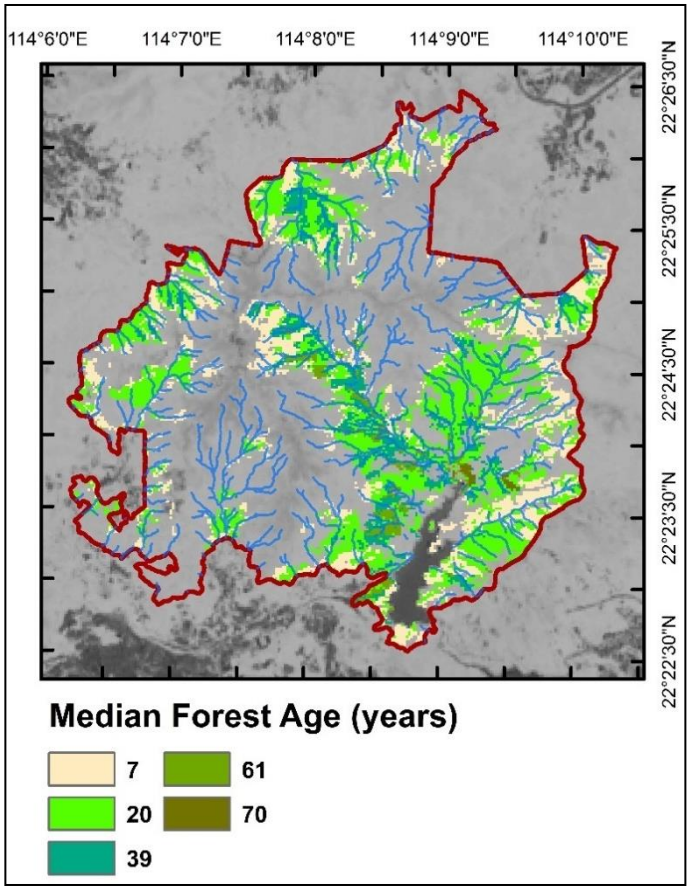

Figure 4-3: Age of different forest patches in the study area

4.3. Climate data

Rainfall in Hong Kong from 2012 to 2017 in different months is shown in Table 4-1. It should be noted that during the time of the field survey unusual cold frost event happened in January 2016. Also, the record rainfall during the month of January 2016 was recorded 266.9 mm. this information is important for the analysis of vegetation phenology.

Table 4-1: Monthly average distribution of rainfall distribution in Hong Kong

Month	**Total Monthly Rainfall (mm)**						
	2011	**2012**	**2013**	**2014**	**2015**	**2016**	**2017**
Jan	5.4	42.1	2.4	Trace	41.7	266.9	7.8
Feb	23.7	29.5	1.5	39.5	32	24.8	19.9
Mar	20.5	22.1	130.5	207.6	28.4	148.7	48
Apr	36	294.9	253.8	132.4	64.5	211.4	58.8
May	186.7	277.7	509.3	687.3	513	233.6	399.3
Jun	435.6	261.5	438.6	436.6	302.1	347.4	656
Jul	226.8	467.8	436.3	260.5	406.2	175.9	570
Aug	157.6	149.8	445.4	548.2	143.3	532.7	489.1
Sep	123.1	213	454.2	140.6	87.9	323.1	192.4
Oct	172.4	46.4	2.9	109.8	168.3	624.4	99.6
Nov	86.1	63.9	83.1	31.1	22.8	131.3	31.2
Dec	2.8	56	88.3	44.7	64.3	6.6	X

4.4. Satellite data used

4.4.1. Hyperion satellite image methodology

The main methodology used is shown in Figure 4-4

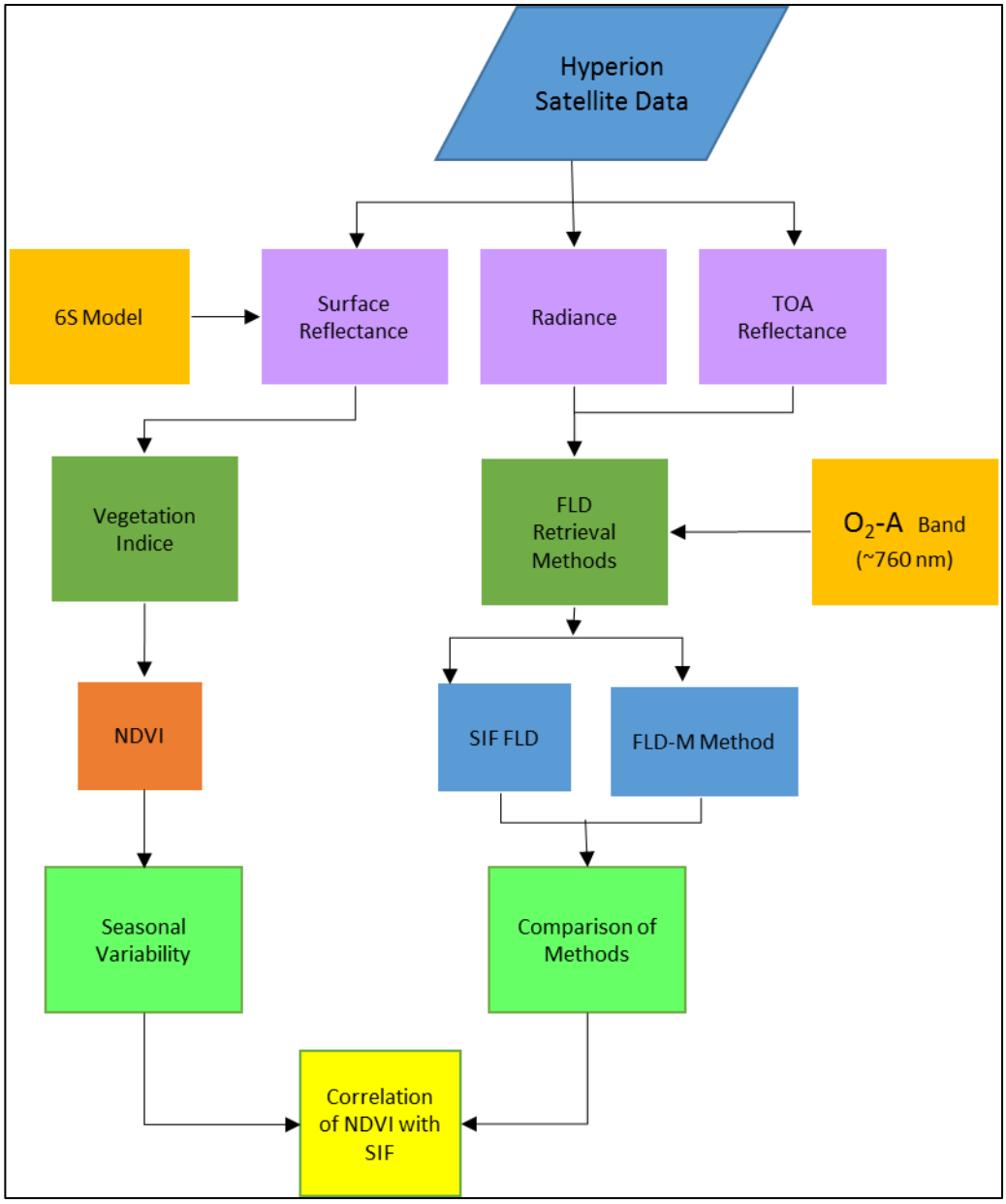

Figure 4-4: Flow chart of the methodology for the Hyperion image analysis

4.4.1.1. Hyperion satellite image acquisition

In this study, analyses are performed on the Hyperion satellite images for the extraction of chlorophyll fluorescence. Ground validation is performed with the help of a field spectrometer. Hyperion satellite images with a ground resolution of 30 m were acquired over the Hong Kong study area. The EO-1's Hyperion sensor equatorial crossing time is around 10 am. It follows the same WRS2 system as Landsat 7. The acquisition times are only 1 minute apart. The swath width of Hyperion compared with Landsat is shown in Figure 4-5. Hyperion EO-1 is a tasking spacecraft, meaning the images acquired are driven by a schedule determined by the user's Data Acquisition Requests (DARs). The requested images can be downloaded from the USGS Earth Explorer website. EO-1 was designed as a technology demonstration mission; thus various spacecraft constraints limit the amount of data that can be collected. EO-1 command centre retrieves cloud predictions from NOAA-NCEP every 6 hours and uses those to determine when to task the upcoming 24 hours of requests. After confirming from their webserver the next cloud-free dates and comparing it with the Hong Kong Observatory cloud free predictions, acquisition request was submitted every time there was a probability and coincident field survey was conducted. From 6th August 2015 to 2nd March 2016 a total of eight images were acquired over Tai Mo Shan Country Park region of Hong Kong. Details of all Hyperion satellite images over Hong Kong region from 2012 to 2016 are shown in Table 4-2.

Table 4-2: Processed satellite images of Hyperion with low cloud cover.

	Gregorian Date	Julian Day	Cloud cover	Target Path	Target Row
1	3-Nov-12	308	40%	121	44
2	9-Mar-13	68	10%	121	44
3	3-Dec-13	337	20%	121	44
4	22-Sep-14	265	20%	121	44
5	8-Oct-14	281	20%	121	44
6	14-Feb-15	45	30%	121	44
7	17-Apr-15	107	20%	121	44
8	6-Aug-15	218	20%	121	44
9	13-Sep-15	256	20%	121	44
10	2-Oct-15	275	20%	121	44
11	18-Oct-15	291	20%	121	44
12	28-Nov-15	332	20%	121	44
13	4-Feb-16	35	20%	121	44
14	9-Feb-16	40	20%	121	44
15	2-Mar-16	62	20%	121	44
16	26-Aug-16	239	10%	121	44
17	2-Nov-16	307	20%	121	44

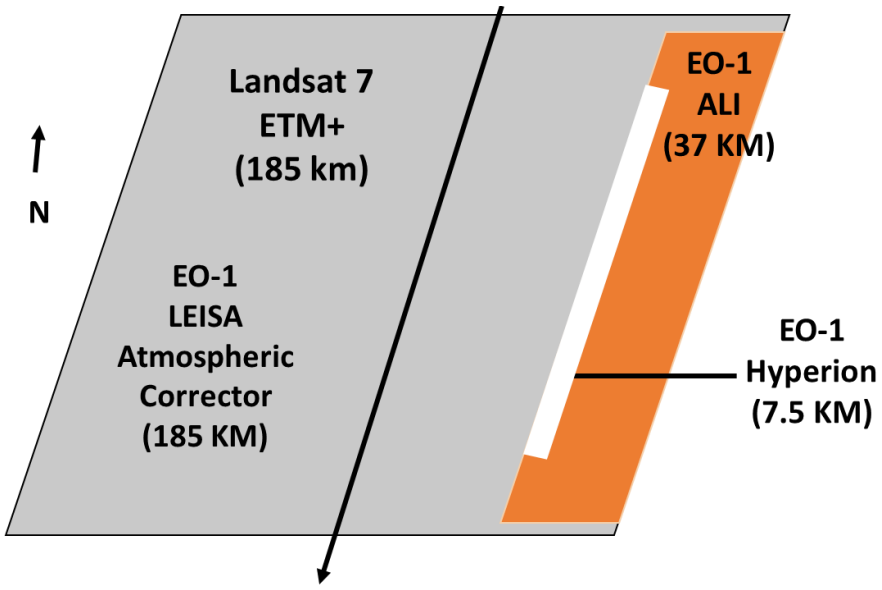

Figure 4-5: Hyperion satellite swath width in comparison with Landsat and ALI

Figure 4-6 shows the field sample points acquired over Tai Mo Shan Country Park region acquired by Hyperion satellite images. Swath with of EO-1 Hyperion is 7.5 km.

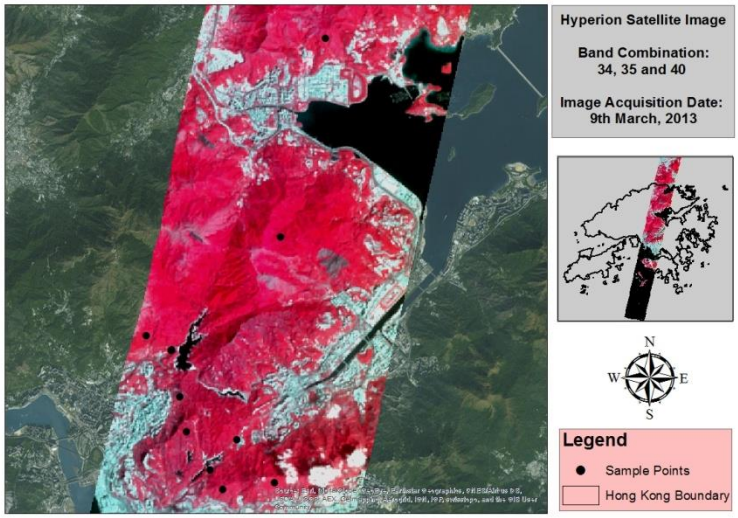

Figure 4-6: Hyperion scene acquired over the study area on 9th March 2013

4.4.1.2. Hyperion band specifications

There are 220 unique spectral channels collected with a complete spectrum from 357 - 2576 nm. The Level 1 Radiometric product has a total of 242 bands, but only 198 bands are calibrated. Because of overlap between the VNIR and SWIR focal planes, there are only 196 unique channels. The calibrated channels are 8-57 for the VNIR, and 77-224 for the SWIR. The reason for not calibrating all 242 channels is mainly due to the detectors' low responsivity. The digital values of the Level 1product are 16-bit radiances and are stored as 16-bit signed integers. The SWIR bands have a scaling factor of 80, and the VNIR bands have a scaling factor of 40 applied. The units are W/m^2 SRμm. VNIR L = Digital Number / 40 SWIR L = Digital Number / 80

The SNR for Hyperion is 190 to 40 as the wavelengths increases. The primary focus was to detect the SIF using O_2A and O_2B band so Bands 25 to Band 45 ranging from 599.8nm to 803.3 nm were selected for the final processing.

4.4.1.3. TOA reflectance and 6S model

The Hyperion image was converted into respective radiance, and TOA radiance for the retrieval of fluorescence and then the atmospheric correction model 6S was applied to derive the vegetation indices. Nazeer et al (2014) showed that the atmospheric correction model 6S gave the best results over all surfaces in the Hong Kong region.

For inputs to the 6S model, information on solar zenith angle (θ_s), solar azimuth angle (φ_s), sensor zenith angle (θ_o), sensor azimuth angle (φ_o), and image acquisition date and time were extracted from the image metadata file, while values of WV and AOD were retrieved from MODIS Terra Daily Level-3 (1° × 1°) global atmospheric product (MOD08_D3.051) Columnar ozone (O3) data were retrieved from the OMI Daily Level-3 (0.25° × 0.25°) global gridded product from **http://gdata1.sci.gsfc.nasa.gov/daac-bin/G3/gui.cgi**? instance_id=omi.

For atmospheric correction, the central wavelength for each band is required. This band can be found in the ENVI header file (*.hdr). Table 4-3 shows all the parameters of the Hyperion image necessary to perform atmospheric correction using the 6S.

Table 4-3: Parameters for the 6S atmospheric correction of Hyperion images

Parameters	3-Nov-12	9-Mar-13	3-Dec-13	22-Sep-14	8-Oct-14	14-Feb-15	17-Apr-15	6-Aug-15
Sensor	Hyperion							
Image time [GMT hd]	2.35	2.25	2.03	1.77	1.72	1.58	1.47	1.32
θ_s	45.49	43.24	54.63	42.51	45.80	57.08	43.53	44.96
φ_s	143.13	124.25	142.18	115.90	123.55	124.14	98.924	88.27
θ_o	-7.70	-10.55	-9.75	-2.32	-6.36	-1.68	-6.10	-3.68
φ_o	98.0	98.0	98.0	98.0	98.0	98.0	98.0	98.0
Water vapor [g/cm^2]	3.0	2.0	2.25	4.0	3.0	3.0	3.0	4.5
Ozone [cm-atm]	0.30	0.30	0.20	0.30	0.30	0.30	0.30	0.30
Aerosol model	Continental							
AOD at 550 nm	0.26	0.50	0.34	0.41	0.90	0.58	0.50	0.26

4.4.1.4. Hyperion O_2A band SIF retrieval method

Two FLD methods were used for the retrieval of SIF from Hyperion images. One is the original FLD method presented by (Plascyk, 1975) and the other one presented by (Raychaudhuri, 2014a) for Hyperion satellite images. Details of both methods have been explained in Chapter 4 section 4.7 and 4.7.4. Before applying both FLD methods, TOA radiance was calculated from Hyperion images after performing the preprocessing task. The O_2A oxygen absorption band 760 nm was used as the reference band for SIF retrieval.

Selection of sensor bands for the retrieval of fluorescence depends upon the spectral resolution of the sensor because spectral resolution strongly influences the absorption band observed spectral shape.

The SIF retrievals were conducted with FLD as shown below in Eq 4.1 (Plascyk, 1975).

$$\mathbf{F} = \frac{\mathbf{L\downarrow\lambda out\ x\ L\uparrow\lambda in - L\uparrow\lambda out\ x\ L\downarrow\lambda in}}{\mathbf{L\downarrow\lambda out - L\downarrow\lambda in}} \qquad \text{Eq 4.1}$$

In the above equation, $L\uparrow$ is the upwelling solar radiance reaching the sensor λ_{out} and λ_{in} is the wavelength outside and inside the oxygen absorption band at 760 nm. Whereas $L\downarrow$ reference to the solar irradiance and its respective wavelength inside and outside of Oxygen Absorption band.

In addition to the FLD method, a modified FLD method (FLD-M) was tested for its ability to deliver improved SIF estimates by cancelling out atmospheric scattering. This is especially important over Hong Kong where high levels of AOD and water vapour are common. Although a standard atmospheric correction using 6S model was initially applied to the images, its testing over Hong Kong showed up to 10 % difference in surface reflectance from ground measurements. Thus, decoupling of the weak fluorescence signal from atmospheric effects may still be difficult. FLD-M is based on Barun Raychaudhuri (2014), where radiation in the O_2A band is compared to its adjacent bands on either side of it, for vegetated and non-vegetated surface respectively. Thus, it uses the ratio of radiation of the O_2A band and bands outside the O_2A bands, from both vegetated and non-vegetated surfaces. A non-vegetated surface accounts for path radiance and surface reflectance whereas a vegetated region includes, in addition, the contribution of chlorophyll fluorescence.

However, an assumption is made that the fluorescence wavelength reaching the sensor is a linear combination of incident radiance reflected from the object. Thus, by calculating F (Equation 4.1) for both vegetated and non-vegetated surfaces, atmospheric parameters can be neglected because at sensor, if vegetated and non-vegetated targets are close enough, atmospheric effects will cancel out. Also, the path radiance will be equal in both

cases (Raychaudhuri, 2014). The final SIF formula using FLD-M method is shown in Equation 4.2.

$$Fm = Fv - Fnv \qquad \text{Eq 4.2}$$

where Fv is the SIF FLD SIF from the vegetated surface, Fnv is the SIF FLD SIF from the non-vegetated surface and Fm represents SIF FLD-M SIF. While it is known that Hyperion images often have a low signal to noise ratio (SNR), especially at low sun angles (Kruse et al. 2003), the tropical location of the study area and avoidance of the winter season for image acquisition is deemed to have minimized this problem.

4.4.1.5. Hyperion NDVI band selection

For the calculation of NDVI surface reflectance, the6S model was applied. The NDVI formula was used as discussed in Eq 4.3 by Damm et al (2015)

$$\boldsymbol{NDVI} = \frac{\mathbf{R_{750} - R_{685}}}{\mathbf{R_{750} + R_{685}}} \qquad \text{Eq 4.3}$$

Wide variation in the estimated values of fluorescence emission may occur, depending on the time of year, the situation of measurement (ground, air or space-based), methodology (simulation and spatial or temporal averaging) and the type of sensor involved. The present work has obtained fluorescence data of comparable numeric ranges for different years and seasons from Hyperion images. The obtained results are within the range suggested by previously reported values.

4.4.2. Planet satellite data

4.4.2.1. Planet satellite image acquisition and pre-processing

Planet satellite images from September 2016 to January 2018 were downloaded from www.planet.com and processed. Available cloud-free images of every month were acquired and preprocessed. Planet satellite image details are given in Table 4-4.

Table 4-4: Characteristics of Planet satellite image

Orbital Characteristics	Sun Synchronous Orbit
Orbit Altitude	475 km
Inclination	98°
Latitude Coverage	--81.5° to +81.5°
Crossing time on equator	9:30 to 11:30 am
Spectral Resolution	Blue: 455 -515 nm
	Green: 500 - 590 nm
	Red: 590 - 670 nm
	NIR: 780 - 860 nm
Spatial Resolution	3.5 to 4 m
Radiometric Resolution	12-bit
Temporal Resolution	Daily
Swath Width	24.6 km x 16.4 km

4.4.2.2. Planet satellite image NDVI

Atmospherically corrected images were acquired for the processing of Planet data. Planet data scenes are atmospherically corrected to TOA reflectance using the 6S model. After creating NDVI images of all the dates, a mosaic of all the images was created for every scene. The mosaiced image was then subset over Tai Mo Shan region, and a total of 30 NDVI mosaic images was created. NDVI values were extracted from all scenes using field survey points of different woody vegetation species and grassland. The average NDVI value of every month was analysed (Figure 4-7).

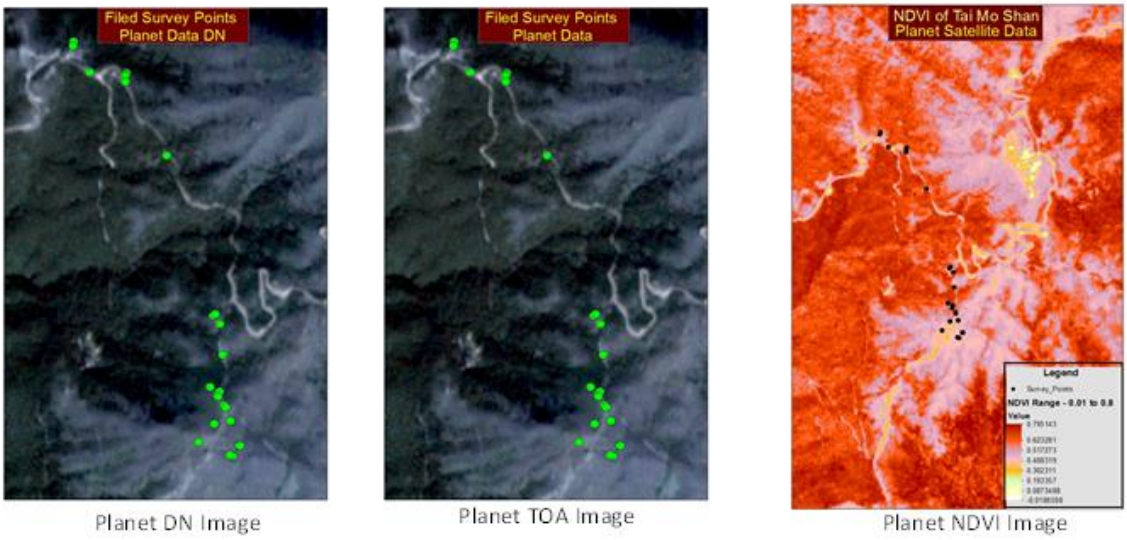

Figure 4-7: Planet image NDVI with grassland and shrubland survey points

4.4.2.3. Pure grassland field survey points

The NDVI was extracted from pure grassland field survey points (Table 4-5)

Table 4-5: Grassland field survey points used for the extraction of NDVI values from the Planet satellite image

No of Observation	Vegetation Cover	Latitude	Longitude	Altitude (m)
1	Grass 1	22.41214	114.11779	728
2	Grass 2	22.4115	114.11899	715
3	Grass 3	22.41144	114.11897	719
4	Grass 4	22.40642	114.12105	749
5	Grass 5	22.40492	114.12101	756
6	Grass 6	22.4045	114.12137	757
7	Grass 7	22.4042	114.12112	XXX
8	Grass 8	22.4038	114.12077	770
9	Grass 9	22.4037	114.12168	760
10	Grass 10	22.4037	114.12168	XXX
11	Grass 11	22.4037	114.1217	752
12	Grass 12	22.4035	114.12148	760

4.5. Methodology flow chart for field measurements

Methodology for field spectrometer fluorescence and indices is shown in Figure 4-8

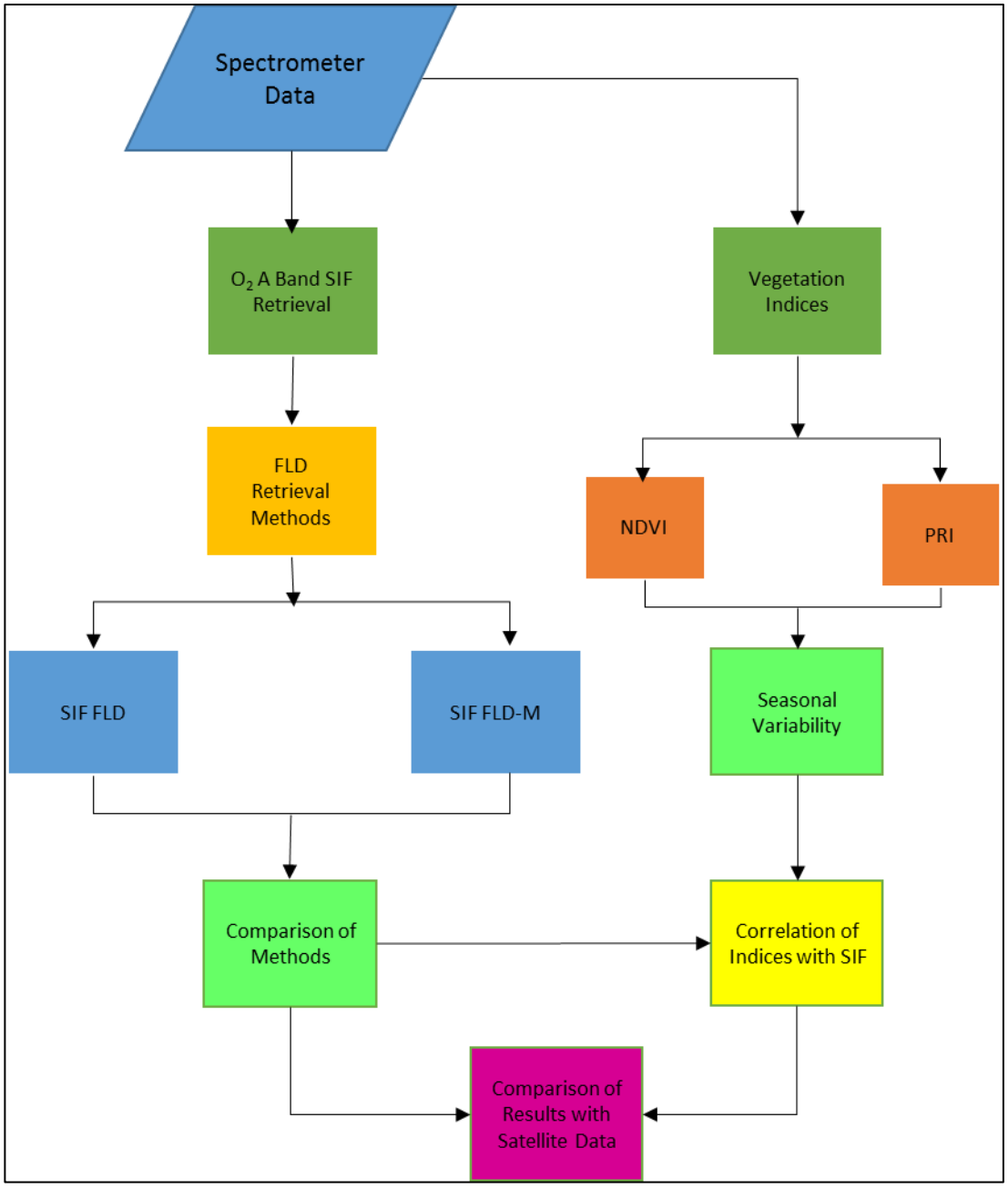

Figure 4-8: Flow chart of SIF retrieval derived from the in-situ spectrometer

4.5.1. Field spectrometer specifications.

Two different field spectrometers were used in this study to collect vegetation spectra over different vegetation species.

4.5.1.1. CropScan MSR-16 spectroradiometer

From May 2015 to March 2016, field spectra were collected at different sites of Hong Kong Country Parks: Kowloon reservoir and Shing Mun Country Parks. Four different vegetation spectra of a broadleaf tree were collected along with water and grasses. Within the specified timespan, SR was collected with the help of Cropscan MSR-16R Multispectral Radiometer (MSR). The purpose was to collect the vegetation spectra to see the trend in vegetation indices over the period to asses vegetation stress (Table 4-6).

Table 4-6: CropScan MSR-16 band specification

Band	Wavelength (µm)	Central Wavelength (µm)
Blue	0.457 - 0.525	0.491
Green	0.525 - 0.597	0.561
Red	0.633 - 0.691	0.662
NIR	0.760 - 0.906	0.833

At all sites 10 spectra were collected for each sample. Field survey dates for spectrometer is shown in Table 4-8. In the final analysis an average value was used to calculate NDVI from each site.

Figure 4-9: MSR-16 field data collection at Kowloon reservoir (left) and Shing Mun Country Park (right)

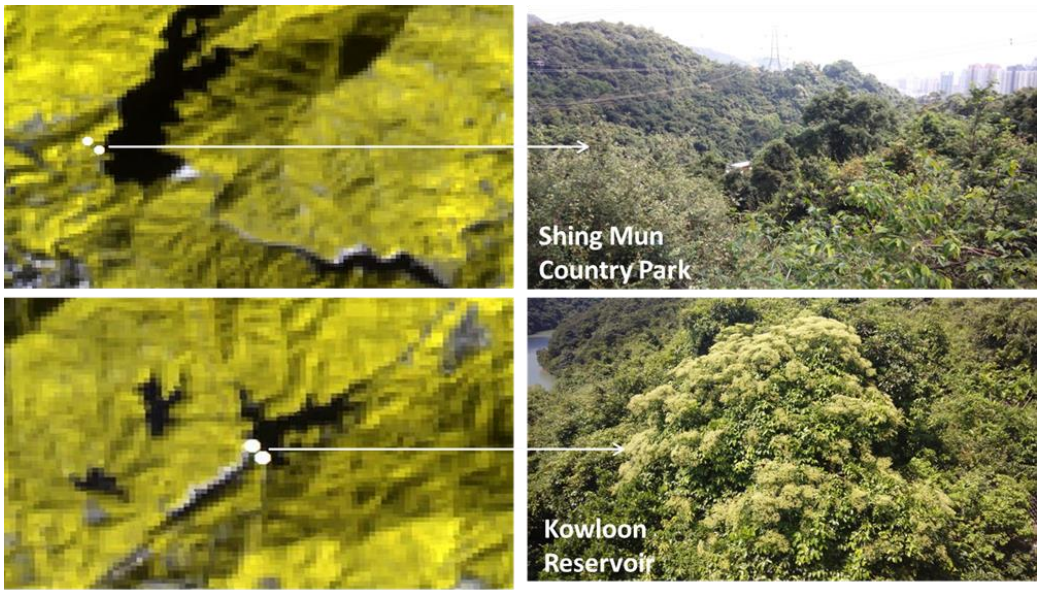

Figure 4-10: Sample site from the satellite image (left) and from the field location (right)

4.5.1.2. Hyperspectral radiometer

RAMSES-ARC spectrometer data from TriOS were used in this study for the measurement of vegetative spectra. The RAMSES Spectrometer data were used for the collection of sample points on 2nd March 2016 in Shing Mun Country Park and Kowloon reservoir and continuous field survey was later shifted to Tai Mo Shan Country Park for continuous monitoring of grassland in Tai Mo Shan region, which was selected because it has homogenous grassland patches. The TriOS Spectrometer is a stand-alone highly integrated hyperspectral radiometer for the UV and VIS spectral range. A battery pack with WLAN interface for the use of TriOS sensors, with Pocket-MSDA offering web server access via WLAN was used. The pocket MSDA is controllable by any laptop, tablet or smartphone with a web browser. Mobile phone WIFI was used with Pocket Power G2 for connecting with the web browser to collect spectral readings. Technical Specification of TriOS Spectroradiometer is given in Table 4-7.

Table 4-7: Technical specification of TriOS spectroradiometer

TriOs Spectrometer Specification	
Optical Detail	
Range of Wavelength	320 nm to 950 nm
Spectral Sampling	3.3 nm
Accuracy	0.3 nm
Channels useable	190
Saturation at 500 nm	1 $Wm^{-2}nm^{-1}sr^{-1}$
FOV	7^0 in air
integration time	4 ms to 8 sec
Data interface (Telemetric)	RS - 232 or Serial Bus
Power	1.5 to 11 VDC
	0.85 W (during data acquisition
Connection	5 pin male connectors
Size	4.7 cm x 29.7 cm
weight	1 kg
Depth	300 m

4.5.2. Field sampling points

Field observations were performed in three different combinations in Tai Mo Shan on different dates (Table 4-8).

- Seasonal observation through a continuous collection of vegetation spectra in different months
- Diurnal observation by taking a reading after every 15 min over a selected grassland patch (for two dates)
- Morning and evening observation (for two dates for two different vegetation species) To ensure about the accuracy about the sample points we consider the following points:

To collect species richness data: Considering the heterogeneity of the landscape and accessibility, it was difficult to find representative stands through random selection, therefore, a stratified random sampling method was used to select plot locations. All the plots were grouped into the five age categories defined by time since recovery (forest since 1945, forest since 1963, forest since 1989, forest since 2001, and forest since 2014). Plots were set up at an altitudinal interval of 200 m, with further considerations for aspect (N, NE, E, SE, S, SW, W and NW), and slope (flat, gentle, moderate and steep), whenever possible. In total, the plots occupy 1.12 ha at elevations ranging from 205 m to 822 m (Abbas, Nichol, Zhang, & Fischer, 2019).

To collect Spectrometer Data: For grassland we selected the homogenous plot. For shrubs we collected points which were dispersed throughout our study area.

Table 4-8: Dates of the spectrometer data acquisition

No	Field Survey Conducted
1	30-May-15
2	4-Jun-15
3	18-Aug-15
4	5 Sept 2015
5	18-Oct-15
7	25-Nov-15
8	9-Feb-16
9	2-Mar-16
13	31-May-17
14	19-Oct-17
15	23-Nov-17
16	3-Dec-17
17	10-Mar-18
18	17-Jun-18
19	22-Sept-18

The schematic diagram of field observation methodology is presented in Figure 4-11

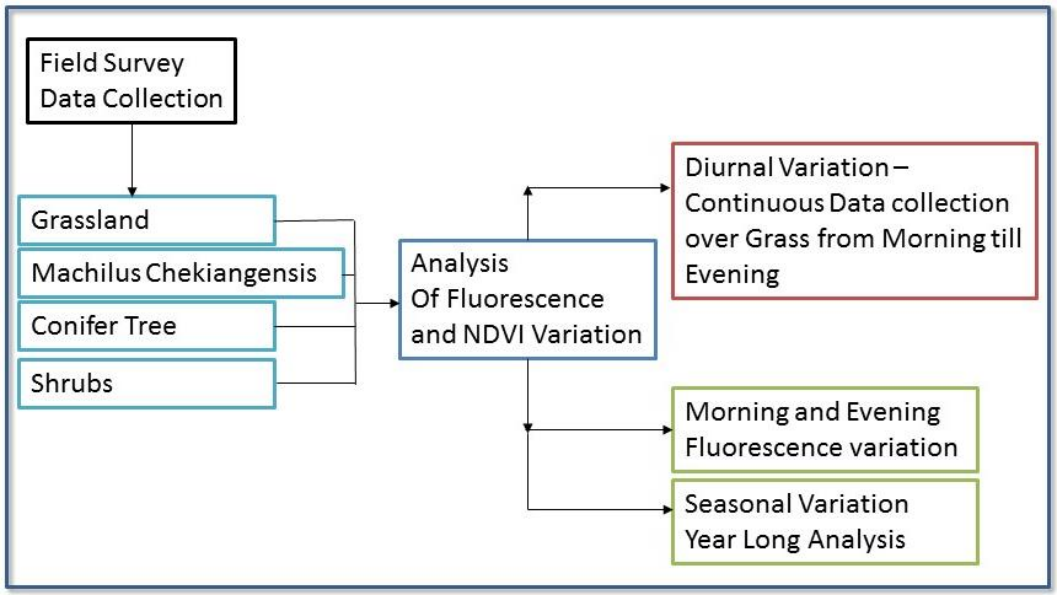

Figure 4-11: Fluorescence and NDVI analysis using field survey spectrometer

4.5.3. Spectrometer field survey experimentation setup

In this study, field measurements were taken between May 2017 to Sept 2018 in different seasons over 26 different vegetative sample points. The main vegetative cover types under observation were grassland, secondary forest dominated by *Machilus chekiangensis*, and Coniferous trees and shrubs in the Tai Mo Shan Country Park. All readings were taken under natural sunlight in the clear sky conditions. For the retrieval of irradiance values, a white reference was used with every observation. The Top of Canopy (TOC) radiances from the spectrometer were collected. Three experiments were performed during field observations. Continuous field observation over one sample point was performed on two dates. TOC radiances were collected from 10:00 am till 2:00 PM to see the variation in the fluoresce value from morning till evening. Secondly, morning and evening values were collected for different vegetative species on two separate dates. Monitoring of vegetation species was performed by collecting data in different months to see the seasonal variations. Both TOC radiance and the irradiance from the white reference (FLD

principle) were used to retrieve the estimated fluorescence. The Barun Method for the retrieval of SIF was also examined using the spectrometer data. The Oxygen Absorption band O_2A at 760 nm was used to retrieve SIF from the narrow band of 3 nm of TIROS Spectrometer. The 3 nm FWHM of the TIROS spectrometer is too broad for the retrieval of O_2B oxygen absorption band at 685 nm which has very narrow band depth, hence retrieval of O_2-B fluorescence was not possible using this spectrometer (Meroni et al., 2009).

The main objective of the fieldwork was to find the seasonal variation of NDVI and SIF of grassland and *Machilus spp*. which is the dominant forest species in Tai Mo Shan throughout the year. Second object was to to find the diurnal variation of grassland in Tai Mo Shan Country Park. After taking this reading aim was to develop the relationship between NDVI and SIF in the grassland region and monitoring the changes in SIF and NDVI in the morning and afternoon in both grassland and forest.

Integration Time

Integration time is one of the most important aspects to monitor while taking a reading from the field spectrometer, as sensitivity of the acquired data varies at different times (Zhang et al., 2017) One integration time for whole field data collection in a day may saturate the spectrum of some points because of the varying irradiance during the day. Therefore, to reduce signal to noise of the sample taken by spectrometer, the integration time for every point was varied, to produce an ideal spectrum for every point. The irradiance value for each sample point was retrieved with the help of a white reference. Figure 4-12 shows the radiance flux of solar radiation from the white reference

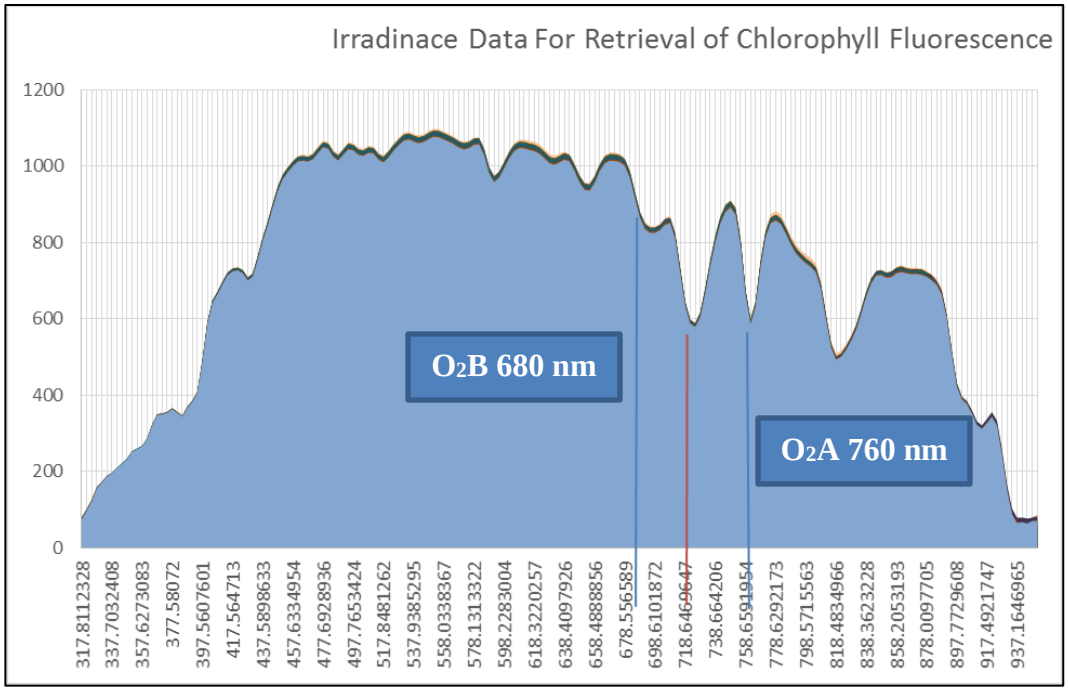

Figure 4-12: Irradiance value collected from the hyperspectral radiometer using a white reference

4.5.3.1. Field survey photos

Figure 4-13: Spectrometer field survey data collection points

Figure 4-14: Photographic evidence of grassland change in Tai Mo Shan Country Park from May 2017 to September 2018 on the same site

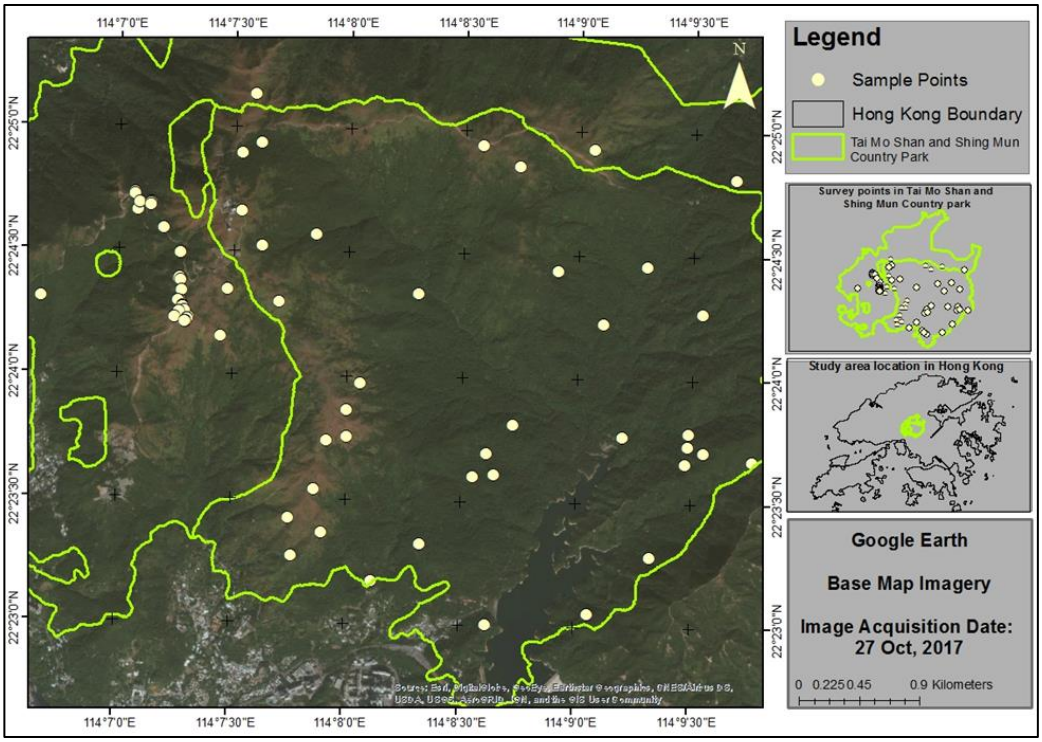

Figure 4-15: Location and distribution of the field observation points

4.5.3.2. Two different spectrometers comparison study

On 2nd March 2016, we used two different spectrometers, the Trios spectroradiometer and the MSR-16 CropScan to monitor the change in spectral properties of vegetation using two different sources.

Figure 4-16: Acquiring vegetation spectra using two different spectral radiometers

CHAPTER 5 RESULTS

5.1. Seasonal variation in Grassland.

5.1.1. Grassland phenology from Planet satellite data

Since Planet satellite data do not have fluorescence retrieval bands, but have higher temporal resolution than Hyperion, Planet data were used for retrieval of monthly NDVI values. This is because it is necessary to observe the detailed phenology of the study area over the year, first using NDVI data, before analysing and understanding the fluorescence observed values from Hyperion satellite images obtained in different months. Planet data phenology (Figure 5-1) is derived from Planet images corresponding to the field survey points over grassland in Tai Mo Shan, over different months. Results show a the similar pattern to the field photographs of green-up and senescence presented in Figure 5-2, namely that low NDVI values are observed from the winter season until spring. The highest NDVI values are observed from May to October, and lowest values in December and January within a year.

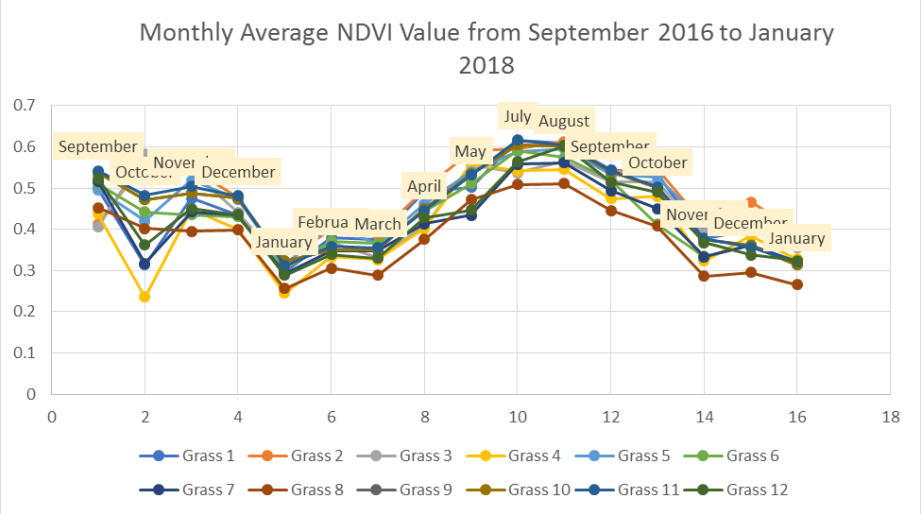

Figure 5-1: Monthly NDVI average values over grassland sample points derived from the Planet satellite images (Sept 2016 to Jan 2018)

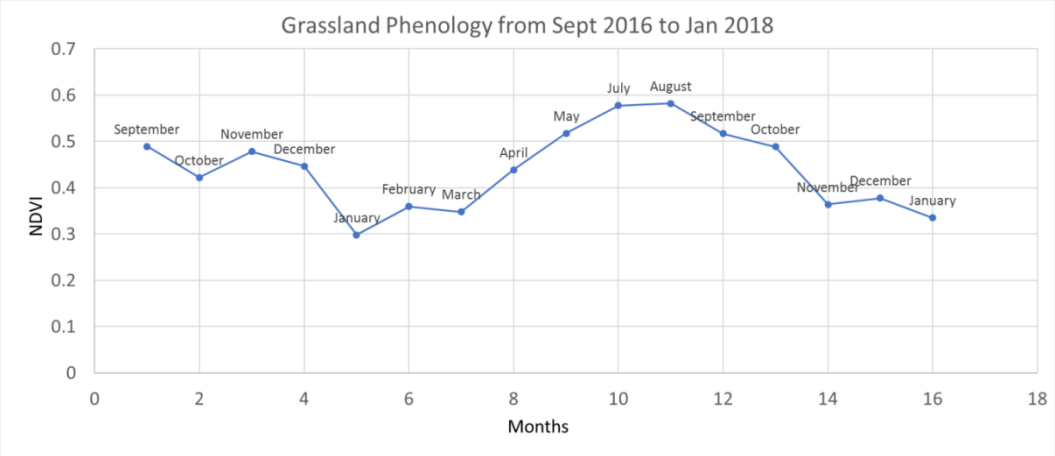

Figure 5-2: Mean grassland phenology derived from the Planet NDVI images (Sept 2016 to Jan 2018)

Figure 5-3 shows all grassland field study points averaged, and represents a summary of the grassland phenological trend, with an interesting dip in NDVI in October/November, followed by recovery in November and December.

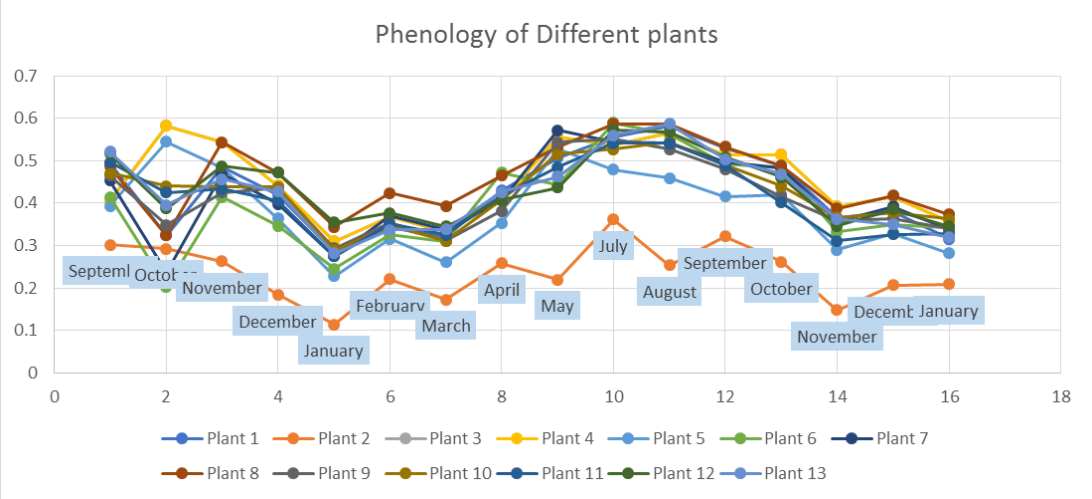

Figure 5-3: NDVI average of shrubland derived from the Planet satellite images (Sept 2016 to Jan 2018)

Similar to grassland, the shrubland NDVI values remain low until, and then start rising up to August. After August, the monsoon season sets in with colder and rainy weather and the NDVI trend declines. Plant 2 which has the lowest overall NDVI value is a frost affected shrub in the Tai Mo Shan Country Park which suffered great damage during the

severe frost of January 2017 (Abbas et al., 2017). Most of its leaves were lost, and the shrub was not in good condition.

5.1.2. Grassland phenology from Spectrometer data

A year-long field experiment using the 3.3 nm hyperspectral spectroradiometer over Tai Mo Shan in grassland (Figure 5-4a) and for the shrub species *Machilus* (Figure 5-4b), suggests that the FLD and FLD-M methods are correlated. As the SIF FLD-M method was adopted to cancel out atmospheric scattering effects, it was not included in this field experiment. Results show that over a year, both NDVI and fluorescence show a strong phenological pattern. Both SIF FLD and NDVI have minimum values in December to March and highest values are observed from May to August (Figure 5-4a). This pattern is also observable in the photographical evidence of grassland of the same area (Figure 4-14). It is notable that *Machilus* shows no significant phenology in NDVI (Figure 5-4b), but very strong phenology is indicated by SIF FLD.

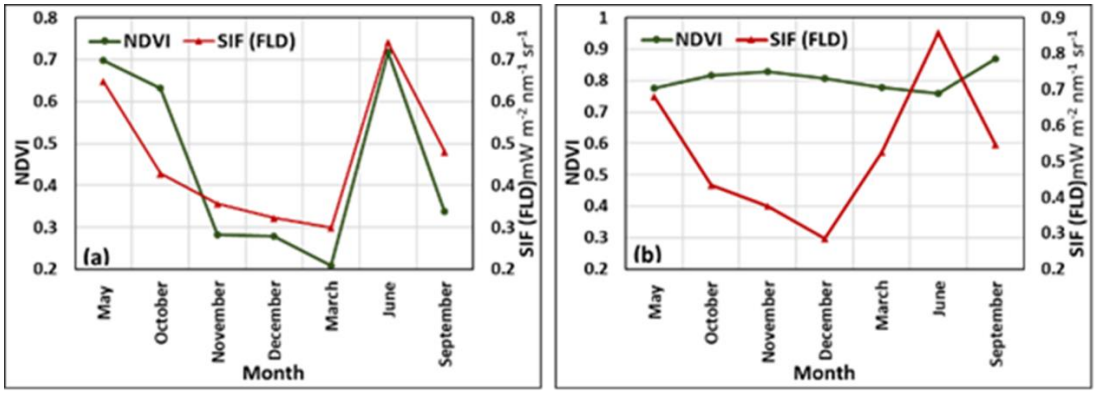

Figure 5-4: Field spectrometer NDVI and SIF response throughout the year for (a) grassland, and (b) shrub

5.1.3. Diurnal variation in SIF and NDVI in grassland

To investigate whether fluorescence and NDVI were responsive and sensitive to diurnal changes over the course of a day, spectrometer observations were acquired over grassland.

Data were collected for two months: June and October 2017. SIF FLD method and NDVI were tested, and results are presented in Figure 5-5. Results showed higher response of SIF FLD to the time of day, compared with the NDVI. The NDVI response showed little variation over the day. This would make the NDVI a good indicator for studies of vegetation condition, because readings from any time of day can be comparable to each other, to indicate change or no change. For example, the seasonal analysis presented in section 5.1.2 showed changes according to season of the year, and these can be considered real changes regardless of time of day of the readings. On the other hand, SIF FLD method respond to sunlight intensity. These results show that not only the time of the year must be considered before retrieving SIF, but also time of the day is important, in order to use SIF as an indicator of health of the vegetation. Figure 5-5 show SIF FLD method retrieved SIF reach maximum SIF values before noon and then decrease afterwards, whereas NDVI values remains same through the day. Overall, the results show that SIF is a better method than NDVI for indicating subtle changes in vegetation health and condition, as the SIF response depends on processes ongoing within the plant tissues as they respond to incident sunlight.

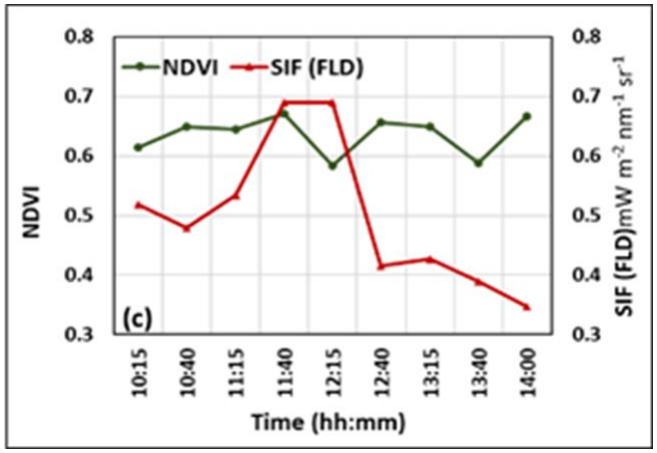

Figure 5-5: Diurnal variation in grassland in October (10:00 am to 02:00 pm)

To explain the diurnal changes in fluorescence values noted above in terms of radiance values, Figures 5-6 and 5-7 show the grassland calibrated radiance upward flux observed by the hyperspectral radiometer for grassland. It should be noted that the oxygen absorption band O_2A at 760 nm played an important role in retrieval of the SIF. A clear dip in the observed radiance at 760 nm is shown in the collected vegetation spectra. That region was used for both the FLD method and FLD-M fluorescence retrieval. Also, it is evident from the observed radiance that in December (Figure 5-6) radiance is higher in the afternoon which might be due to atmospheric factors such as temperature, variation in solar irradiance and the vegetation biophysical properties. However, in March (Figure 5-7), the morning spectra are higher than the afternoon spectra, which may suggest that during the green-up season there is an early response to sunlight, whereas in the senescing season plants make use of higher afternoon temperatures in order to survive.

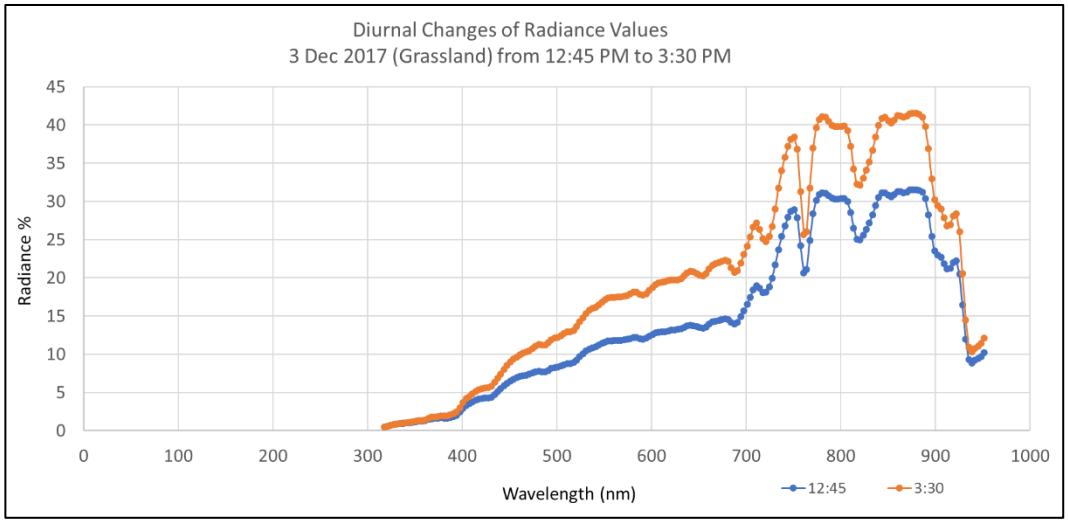

Figure 5-6: Diurnal variation in radiance upward flux of grassland measured using the spectrometer (December 2017).

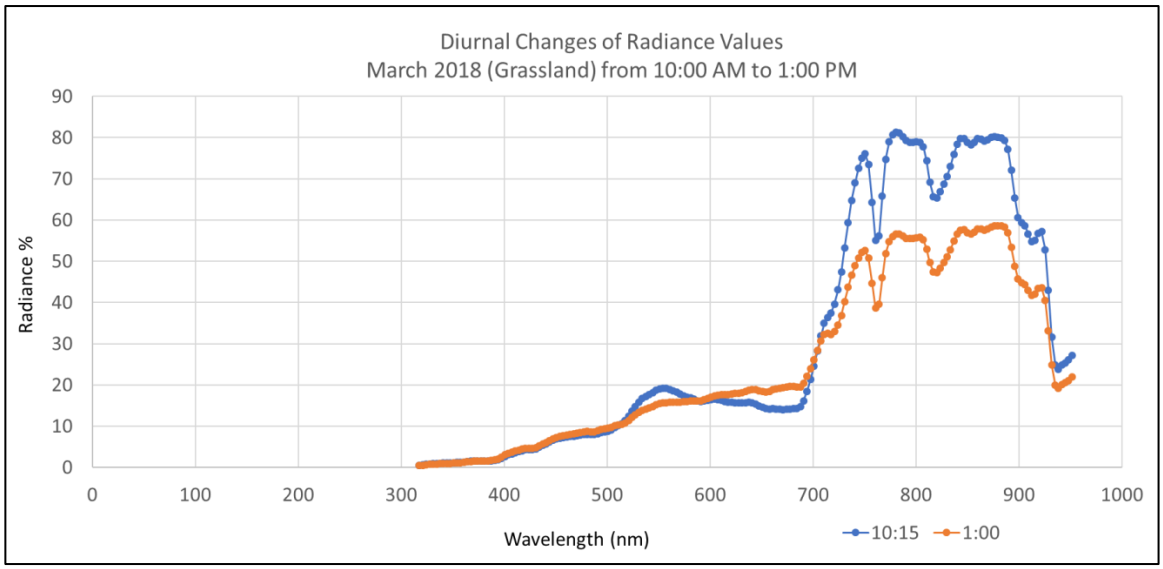

Figure 5-7: Diurnal variation in radiance upward flux of grassland measured using the spectrometer (March 2018)

5.2. Seasonal variation in vegetation structural classes

5.2.1. Relationship between SIF and NDVI with vegetation structural classes

Analyses were performed from fluorescence and NDVI values retrieved over different land cover types in Tai Mo Shan Country Park. Two months were selected, which show the transitional period between senescence and greening up. Figure 5-8 shows the changes

in the NDVI among the different structural stages of vegetation, which gradually decrease from woody vegetation to grassland. However no significant differences in NDVI are observed between forest and exotic plantations in the study area. The bar graphs of plantations and forest (Figure 5-8) show almost similar values of NDVI for forest and plantations in both senescence and green-up seasons. However, fluorescence (Figure 5-8) shows a very significant difference between plantations and forest. The differences in SIF between plantations and forest were quantified by determining the percentage difference, using $(SIF_{plantations} - SIF_{forest})/ SIF_{plantations}$. The SIF derived from the FLD method shows plantations to be 3.5% and 8.7% higher than for forest in October and March, respectively. For the FLD-M method the SIF of plantations is 6.9 % and 9.5% higher than for forests in March and October. Both methods show that the difference is higher in March, the driest season.

The difference is higher in the driest season which is the month of March, and the best segregation between plantations and forest was achieved by the FLD-M method which showed more difference than the FLD method. The FLD-M method also showed more difference between the seasons than the FLD method. Regarding the differences in vegetation response in the greening (March) and browning (October) seasons, the NDVI shows significant differences between the vegetation classes at green-up (in proportion to biomass, with forest/plantations highest and grassland lowest), but the NDVI shows insignificant differences between classes in the browning season. Fluorescence on the other hand shows significant differences between classes in both seasons, with FLD-M in particular showing more differences between the seasons than the FLD method, for all classes.

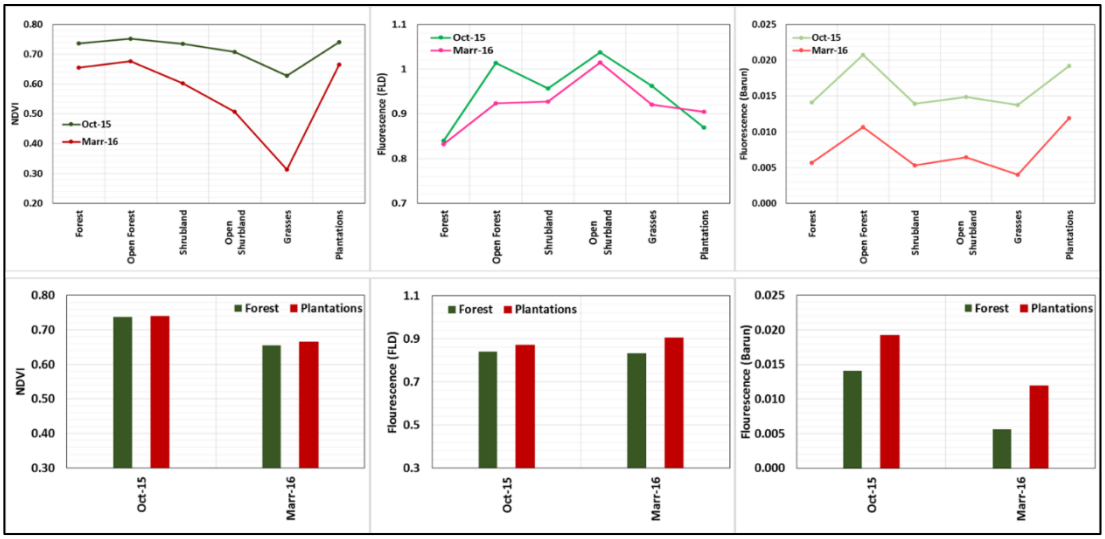

Figure 5-8: NDVI and fluorescence response for the month of March and October over different land cover types

5.2.2. Vegetation structural classes phenology from MSR-16 Cropscan

Continuous monitoring of four vegetated field sites was conducted using the Multispectral MSR-16 Cropscan radiometer, from May 2015 to March 2016 (Figure 5-9). Different combinations of vegetation indices were applied. The pattern of variation in the indices of vegetation spectra corroborate experiments performed using satellite data and the hyperspectral radiometer in Tai Mo Shan region, showing that during the green up season, the vegetation NDVI is higher than the senescence in October. This senescence pattern in October was also observed in the Kowloon reservoir and Shing Mun regions using the hyperspectral radiometer.

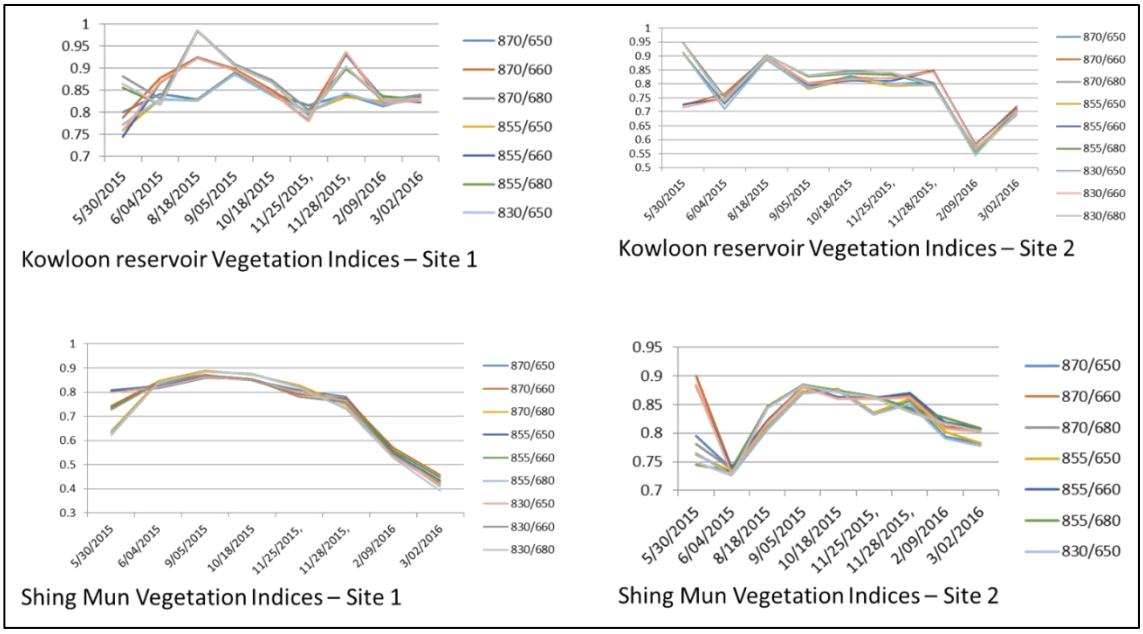

Figure 5-9: Phenological variation of vegetation using spectrometer in Shing Mun and Kowloon reservoir Country Park (2015 to 2016)

5.3. Analysis of species richness and abundance

Comparisons were conducted between the NDVI and fluorescence respectively, and the different woody vegetation types in terms of their species richness and abundance, to examine any differences in NDVI and fluorescence according to forest species composition. This analysis is important because different species of trees and shrubs senescence and green-up at different seasons and this can alter their fluorescence and NDVI values. Species richness represents the number of species present, and abundance refers to the evenness of distribution of individuals among a species in a community.

Figure 5-10 shows the ages of forest species in the study area in terms of richness and abundance. Figure 5-11 shows the correlation between forest species richness and abundance with respect to fluorescence and NDVI response. Results indicate that both FLD and NDVI show good correlation with species richness and abundance, while FLD-

M shows lower correlation. Overall, there appears to be no advantage in using fluorescence methods over the NDVI**,** for analysis of forest species composition.

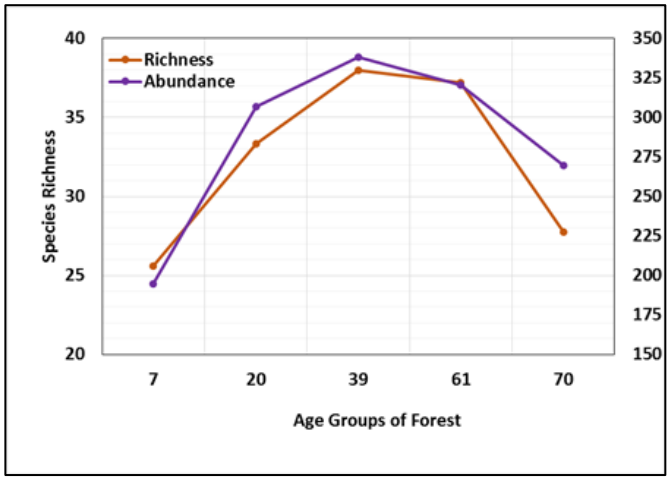

Figure 5-10: Graphical representation of species richness and abundance in Tai Mo Shan Country Park

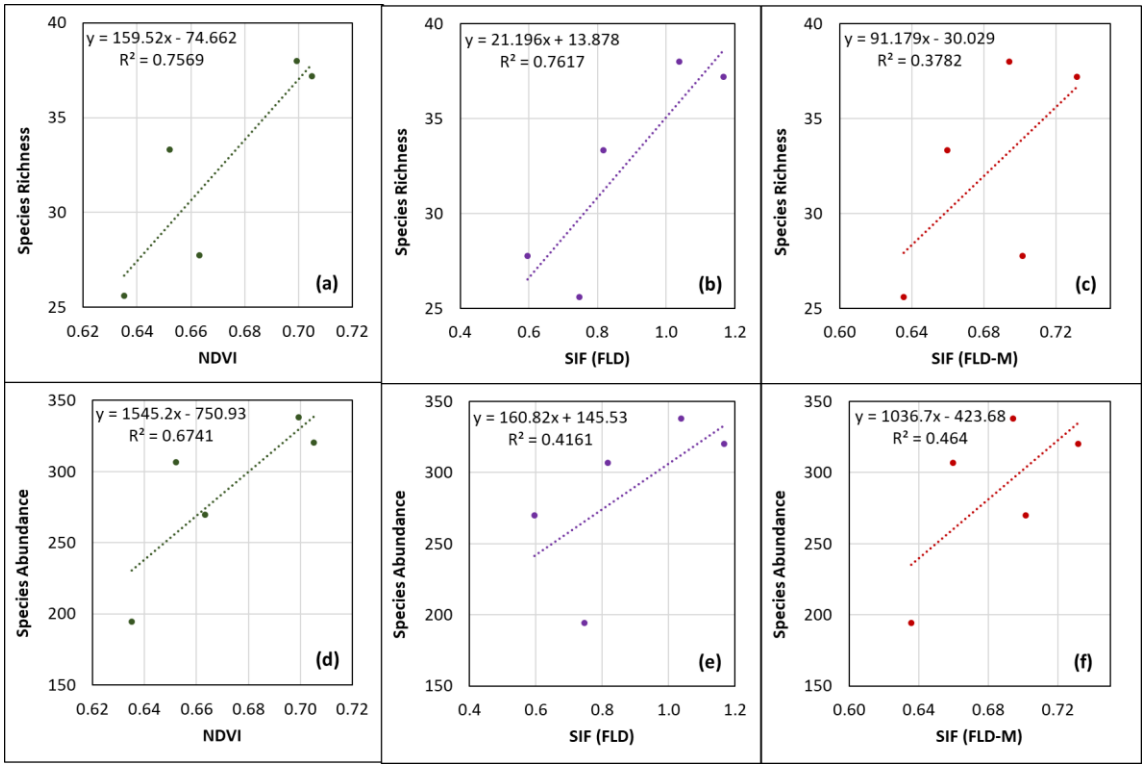

Figure 5-11: Correlation between Species Richness with SIF and NDVI

5.4. Fluorescence and NDVI with respect to forest age classes

Figure 5-12 shows the responses of five different forest age classes at greening and browning seasons. Both NDVI and FLD-M indicate significant and consistent difference between the seasons across all age classes (Fig. 5-12), which is expected due to March being the end of the dry season. The FLD method does not represent these differences. However, the SIF FLD methods shows more difference between the age classes than do the NDVI and SIF FLD-M, with a continuous and large increase in fluorescence emission with age up to 61 years, after which the 70-year forest shows a dramatic fall in response (Fig. 5-12b). This large drop in photosynthetic response between 61-year and 70-year old forest appears unrealistic given the small age difference, as well as the stability of the forest species composition and structure over these age classes (Abbas et al., 2019). The FLD-M method of SIF appears to be the overall best index for representing both the distinction between seasons, as well as among different forest age classes. The age classes represent potentially different levels of carbon sequestration, especially marking a distinct reduction after 60 years of age. Most notably, the FLD method shows less ability to distinguish between seasons for the 5 forest age classes, than either NDVI or FLD-M.

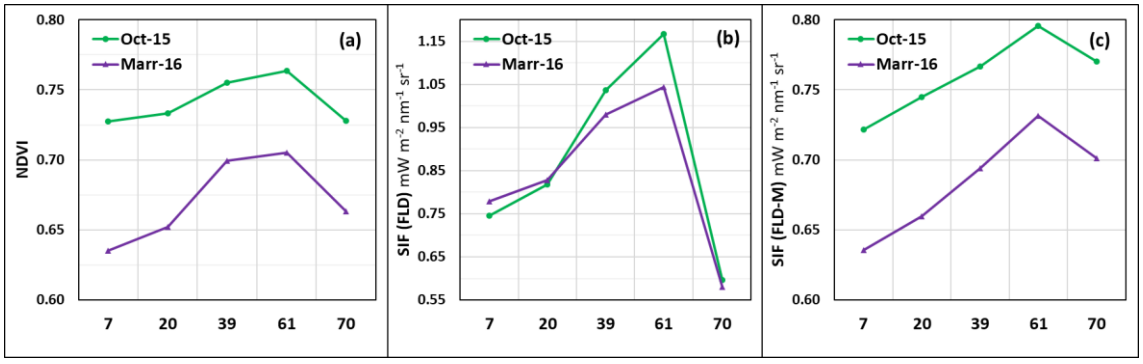

Figure 5-12: Forest age class related to NDVI and SIF

5.5. Hyperion satellite data analysis

5.5.1. NDVI and SIF comparison from Hyperions satellite.

The NDVI and fluorescence values retrieved from the Hyperion satellite image showed very low correlation over the different sample points (Figure 5-13). This is because NDVI remains constant throughout the day whereas fluorescence values showed considerable variation diurnally, as well as seasonally and with respect to different vegetation types. This indicates that fluorescence is a much more sensitive indicator of vegetation growth processes, health and condition, than NDVI.

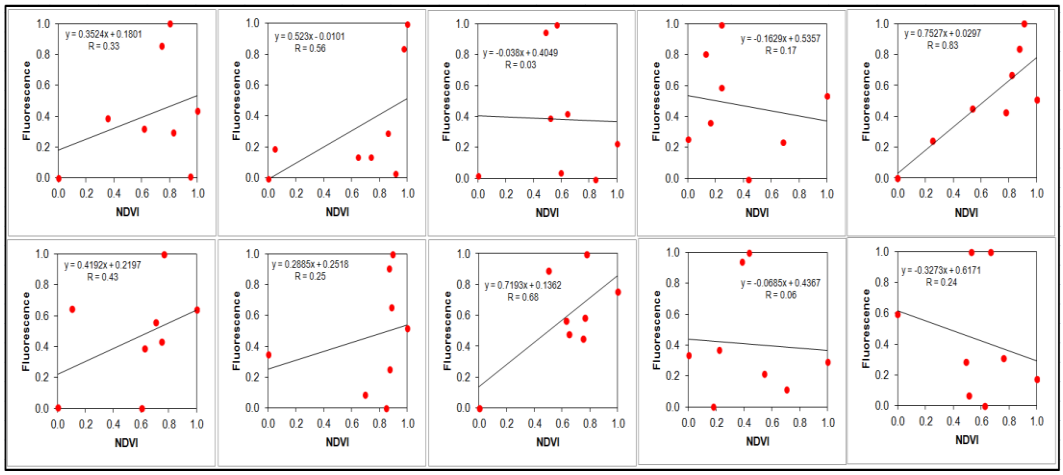

Figure 5-13: Correlation between NDVI and fluorescence derived using O_2A from Hyperion satellite image

5.5.2. SIF retrieval from Hyperion hyperspectral satellite data

Variations in retrieved fluorescence values from both FLD and FLD-M method over different seasons shows that the grassland greening starts from March, with high growth rates lasting until mid-October, followed by senescence from October. Lower fluorescence values are observed until the month of March. March appears to be the transitional period from senescence to greening up of the grassland region. NDVI values

observed from Hyperion suggest the same pattern for FLD-M and FLD methods, where lower values are observed in the period between November to February. March is the driest month but greening of the grassland area starts from March until October. Figure 5-14 shows the FLD method fluorescence images from Hyperion and shows considerable variation for different months.

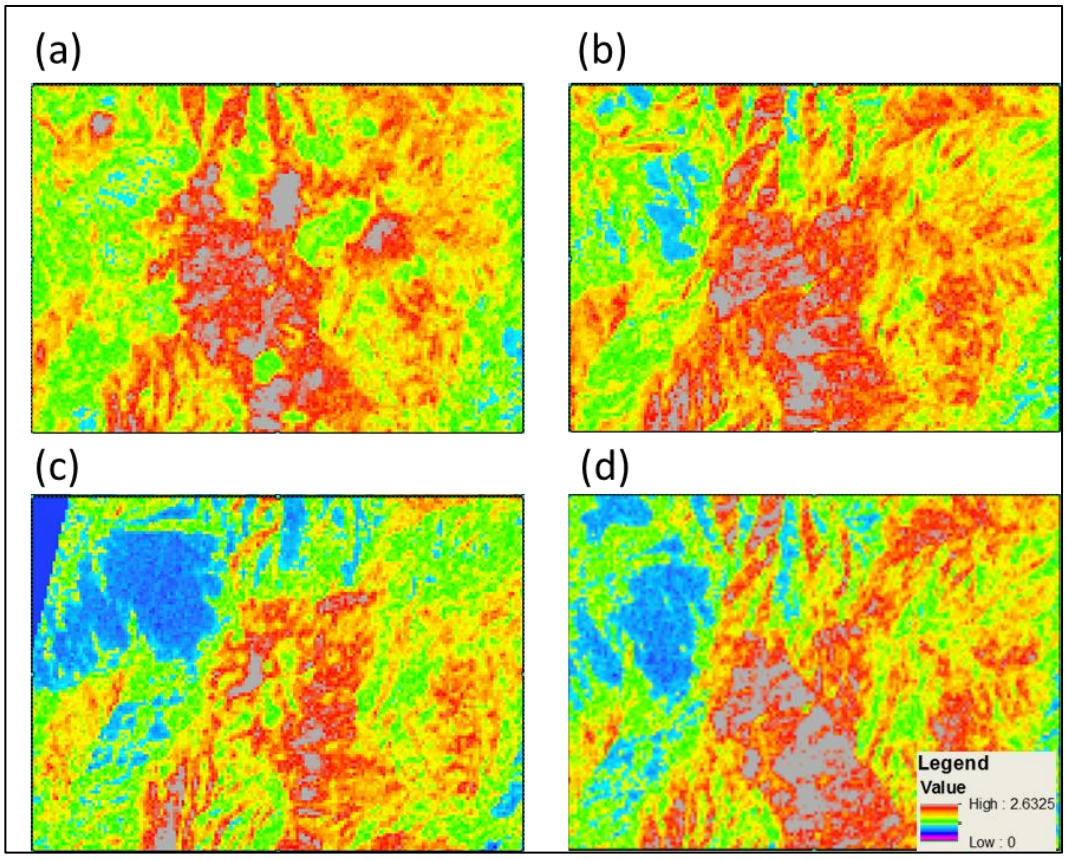

Figure 5-14: SIF (FLD) from the Hyperion satellite images (a) September 2015 (b) October 2015 (c) November 2015 (d) March 2016

5.5.3. Comparison between spectrometer and satellite-based SIF

Comparison between spectrometer derived fluorescence using FLD Method, and Hyperion satellite based fluorescence (Table 5-1 and Figure 5-15), showed a high correlation of 0.91. Although only 3 coincident dates were available, they do show similar values, which indicate a good confidence in the results of the satellite-based observations.

Table 5-1: Comparison of spectrometer and satellite based fluorescence.

Spectrometer Fluorescence	Satellite Fluorescence
0.044	0.022
0.008	0.004
0.022	0.018
Correlation	0.905

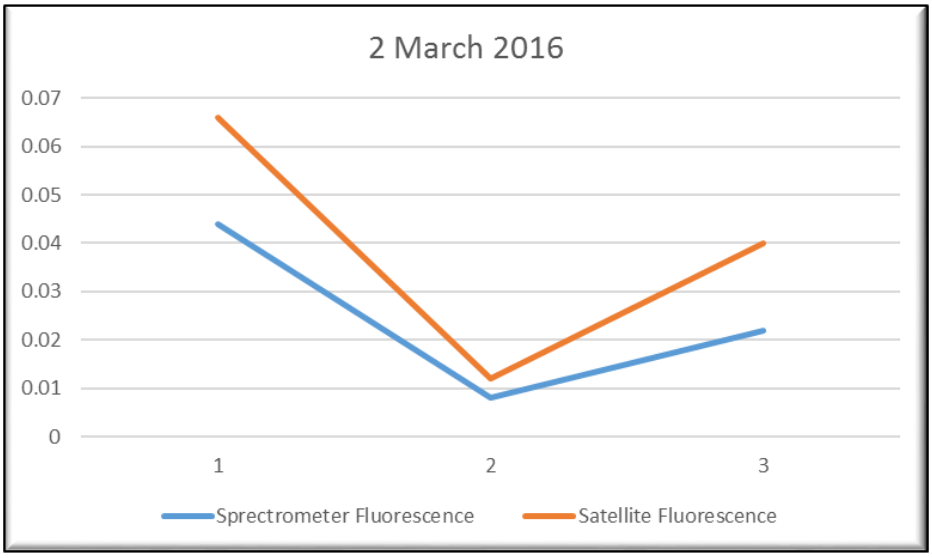

Figure 5-15: Comparison of Spectrometer and satellite based SIF (FLD)

CHAPTER 6 DISCUSSION AND CONCLUSION

6.1. Discussion

The main aim of this research was to examine and recommend a fluorescence-based methodology for measuring the health and condition of the vegetation in Hong Kong's Country Parks. Retrieval of SIF from space-based platforms requires consideration of many parameters to make accurate estimates. In this study, the year-long phenological trend in the vegetation according to seasons, was observed and recorded, by calculating the NDVI using both field-based radiometers, and Planet satellite images over different vegetation sites. This enabled better understanding of change and variability in the study area vegetation, to set in context the fluorescence retrievals from the field-based hyperspectral radiometer and Hyperion satellite data. The study concentrated on, but was not restricted to, grassland as this exhibits greater phenological change over the year, than woody vegetation types.

The phenological pattern observed by the NDVI showed significant differences between the structural vegetation types, with an expected increase in NDVI according to biomass levels, from grassland through to closed forest. However no significant NDVI differences were observed between the exotic plantations and forest. Conversely, the FLD-M method for SIF retrieval showed very significant differences between plantations and forest. The difference was significant in both greening and senescence seasons, but greater in the greening season in March, which also corresponds to the end of the dry season. Whether or not the moisture status of the vegetation plays a role in positively influencing the FLD-M SIF signal, for better distinguishing between plantations and forest, and between the

seasons (ie. greater difference between the seasons as well as between the classes) would require further research. However, it is notable that the SIF FLD and SIF FLD-M retrieval also gave better discrimination between plantations and forest for the end of dry season, and both were better than NDVI in both seasons. Therefore, further research on vegetation moisture status may be useful.

Further evidence that SIF values may be a better measure of vegetation phenology than the NDVI, was obtained from measurements of the shrub species *Machilus chekiangensis*, where both SIF methods showed very strong phenological changes over the year compared to almost no change from the NDVI. Although the grassland sites showed strong phenology for both NDVI and SIF, woody species might not be expected to show much seasonal change. Thus again SIF appears able to measure subtle changes which the NDVI does not show, and these changes may be unrelated to the degree of greenness of the plant leaves. This is supported by Merrick et al (2019) who found that in Amazon forests, fluorescence was more sensitive to photosynthetic activity than to canopy biomass.

In forestry the distinction between different age classes of forest is important for managing the secondary succession of recovering or regenerating forests, as species richness and diversity build up over time, and the oldest forests may be more ecologically stable. In this study the FLD method of fluorescence retrieval showed strong ability to distinguish between different age classes of forest, and significantly better than FLD-M or NDVI. All three methods showed a continuous and significant increase in fluorescence emission with age till 61 years, with decline in the oldest growth forest. However, the differences were much greater with FLD method, which showed the old growth forest with even lower

fluorescence response than all other younger age classes. These observations accord with those of forest ecologists and have significance for climate change studies. For example, Zhou et al., (2015) quantified a relationship between forest age and the carbon sink and found that carbon sequestration gradually increases and peaks at around 22 years and then start declining. He et al., (2012) found a temporal pattern of rapid increase in Net Primary Productivity (NPP) in USA forests at young ages, peak growth in the middle ages, and slow decline in the mature ages. In fact, Ryan et al., (1997) linked the declining patterns of forest growth with a decline in photosynthesis and dry matter production once a canopy achieves a maximum leaf area. Giardina et al., (2018) that showed that forest age and height are both controlling factors of photosynthesis in Amazonian forests. Interestingly, a study of SIF emission in pine plantations in North Carolina found that young plantations stands exhibited a nearly two times higher red fluorescence yield than mature forest plantations due to a photosynthetic stomatal limitation in ageing plantation stands (Colombo et al., 2018).

The vegetation indices NDVI and fluorescence were also examined in terms of diurnal changes in canopy response over the course of a day, in both summer and winter. It was observed that whereas the retrieved NDVI index shows little change over the daylight hours, both fluorescence methods show considerable variability. Whereas FLD-M was similar to NDVI with little diurnal change in winter, both FLD-M and FLD showed very significant diurnal change in summer, with values peaking around 12 noon. The FLD method showed high variability over the day in both seasons. Since the fluorescence values peak at 12 noon, the time in the day when there is maximum solar radiation, and no in early afternoon when the peak temperature is usually reached, the increased SIF

values must be a physiological response to sunlight rather than temperature. Overall this result indicates that SIF is a better measure of vegetation physiological processes in real time, and in this sense, it is more sensitive to vegetation health than NDVI. However, care should be taken when comparing SIF values obtained at different times of day or even at the same time of day in different seasons of the year when sun angle is different. Generally established theory (Meroni et al., 2009) suggests that the chlorophyll fluorescence and photosynthesis processes are negatively correlated in two situations, (i) in low light conditions when plants are healthy, and (ii) in plant stress conditions in full sunlight. This explains the very great differences in SIF response as light conditions change over the course of one day, whereas the NDVI showed little change as it is more dependent on the structure of plant leaves which do not change diurnally. That is why detailed study of fluorescence should be considered for any vegetation stress related study. Otherwise fluorescence relates positively with photosynthesis, even under optimal conditions when plants started to release excess energy in the form of heat instead of fluorescence, and the fluorescence emissions fall because of this.

6.2. Conclusion

In this study using the O_2A absorption band to retrieve fluorescence, along with NDVI from space based and ground-based instruments it is evident that a more complete picture of vegetation processes and the current health status of plants is available by retrieval of fluorescence indices. This study also found that the SIF FLD method was more sensitive than SIF FLD-M method, to diurnal changes in the vegetation canopy and different age classes, but SIF FLD-M was better able to distinguish between different vegetation structural types. This would mean that overall, SIF FLD-M method would be preferable

for detecting long term changes in a vegetation canopy as well as detecting vegetation structural classes. The diurnal sensitivity of FLD method would render it unsuitable for multitemporal studies due to likely differences in incident sunlight onto the vegetation canopy. The overall recommendation for monitoring vegetation in Hong Kong's Country Parks, resulting from this study, Of the two SIF methodologies tested with the Hyperion image data, FLD-M gave more consistent and useful indications of plant health and condition, than the FLD method, which is likely due to its additional compensation for high atmospheric turbidity in the study area. Further research on how vegetation moisture status affects the SIF signal may be useful, in view of forest dieback due to climate change reported in many regions.

Recommendations arising from this study

Although Hyperion was decommissioned in April 2017, there is strong likelihood of more hyperspectral sensors such as the forthcoming FLEX mission. These will have better spatial and temporal resolutions.

It is recommended to conduct continuous monitoring of Hong Kong forested areas, using the SIF FLD-M. SIF methodology along with NDVI, as many natural events occurred during the period of this study, which brought about considerable changes in the study area over a short period of time. In January 2016 a severe frost event affected the Tai Mo Shan Country Park which adversely impacted the vegetation in the study area (Abbas et al., 2017). Frost related stress is predicted to occur more often in future due to climatic warming simulating earlier spring growth. Hong Kong is also prone to severe typhoons such as the super-typhoon of September 2018, which caused serious damage to the young forest and plantations (Abbas et al., 2020). It is recommended to carry out closer

monitoring of environmental impacts on Hong Kong's forested and grassland regions using fluorescence-based methodologies along with NDVI, from both space and field instruments.

REFERENCES

Abbas, S., Nichol, J.E., Fischer, G.A., 2017. Mapping and assessment of impacts of cold and frost on secondary forest in the marginally tropical landscape of Hong Kong. Agric.For.Meteorol.232, 543–549. https://doi.org/10.1016/j.agrformet.2016.10.008

Abbas, S., Nichol, J.E., Fischer, G.A., Sing, M., Irteza, S.M., 2020. Agricultural and Forest Meteorology Impact assessment of a super-typhoon on Hong Kong ' s secondary vegetation and recommendations for restoration of resilience in the forest succession.Agric.For.Meteorol.280,107784. https://doi.org/10.1016/j.agrformet.2019.107784

Abbas, S., Nichol, J.E., Zhang, J., Fischer, G.A., 2019. The accumulation of species and recovery of species composition along a 70 year succession in a tropical secondary forest. Ecol. Indic. 106, 105524. https://doi.org/10.1016/j.ecolind.2019.105524

Alexander Ač, Zbyněk Malenovský, Julie Olejníčková, Alexander Gallé, Uwe Rascher, G.M., 2015. Meta-analysis assessing potential of steady-state chlorophyll fluorescence for remote sensing detection of plant water, temperature and nitrogen stress. Remote Sens. Environ. 168, 420–436. https://doi.org/10.1016/j.rse.2015.07.022

Alonso, L., Gómez-Chova, L., Vila-Francés, J., Amorós-López, J., Guanter, L., Calpe, J., Moreno, J., 2008. Improved fraunhofer line discrimination method for vegetation fluorescence quantification. IEEE Geosci. Remote Sens. Lett. 5, 620–624. https://doi.org/10.1109/LGRS.2008.2001180

Amoros-Lopez, J., Gomez-Chova, L., Vila-Frances, J., Alonso, L., Calpe, J., Moreno, J., Del Valle-Tascon, S., 2008. Evaluation of remote sensing of vegetation fluorescence

by the analysis of diurnal cycles. Int. J. Remote Sens. 29, 5423–5436. https://doi.org/10.1080/01431160802036391

Badgley, G., Field, C.B., Berry, J.A., 2017. Canopy near-infrared reflectance and terrestrial photosynthesis.

Baker, N.R., 2008. Chlorophyll fluorescence: a probe of photosynthesis in vivo. Annu. Rev.PlantBiol.59,89–113. https://doi.org/10.1146/annurev.arplant.59.032607.092759

Brantley, S.T., Zinnert, J.C., Young, D.R., 2011. Application of hyperspectral vegetation indices to detect variations in high leaf area index temperate shrub thicket canopies. Remote Sens. Environ. 115, 514–523. https://doi.org/10.1016/j.rse.2010.09.020

Campbell, P.K.E., Middleton, E.M., Corp, L. a., Kim, M.S., 2008. Contribution of chlorophyll fluorescence to the apparent vegetation reflectance. Sci. Total Environ. 404, 433–439. https://doi.org/10.1016/j.scitotenv.2007.11.004

Census and Statistics Department, 2016. Hong Kong 2016 Population By-census - Key Statistics 8–9. https://doi.org/10.1101/261925

Chance, K. V., Spurr, R.J.D., 1997. Ring effect studies: Rayleigh scattering, including molecular parameters for rotational Raman scattering, and the Fraunhofer spectrum. Appl. Opt. 36, 5224. https://doi.org/10.1364/AO.36.005224

Colombo, R., Celesti, M., Bianchi, R., Campbell, P.K.E., Cogliati, S., Cook, B.D., Corp, L.A., Damm, A., Domec, J.C., Guanter, L., Julitta, T., Middleton, E.M., Noormets, A., Panigada, C., Pinto, F., Rascher, U., Rossini, M., Schickling, A., 2018. Variability of sun-induced chlorophyll fluorescence according to stand age-related processes in a managed loblolly pine forest. Glob. Chang. Biol. 1–17.

https://doi.org/10.1111/gcb.14097

Coops, N.C., 2015. Characterizing Forest Growth and Productivity Using Remotely Sensed Data. Curr. For. Reports. https://doi.org/10.1007/s40725-015-0020-x

Damm, A., Elber, J., Erler, A., Gioli, B., Hamdi, K., Hutjes, R., Kosvancova, M., Meroni, M., Miglietta, F., Moersch, A., Moreno, J., Schickling, A., Sonnenschein, R., Udelhoven, T., van der Linden, S., Hostert, P., Rascher, U., 2010. Remote sensing of sun-induced fluorescence to improve modeling of diurnal courses of gross primary production (GPP). Glob. Chang. Biol. 16, 171–186. https://doi.org/10.1111/j.1365-2486.2009.01908.x

Damm, A., Erler, A., Hillen, W., Meroni, M., Schaepman, M.E., Verhoef, W., Rascher, U., 2011. Modeling the impact of spectral sensor configurations on the FLD retrieval accuracy of sun-induced chlorophyll fluorescence. Remote Sens. Environ. 115, 1882–1892. https://doi.org/10.1016/j.rse.2011.03.011

Damm, A, Guanter, L., Paul-Limoges, E., Van Der Tol, C., Hueni, A., Buchmann, N., Eugster, W., Ammann, C., Schaepman, M.E., 2015. Far-red sun-induced chlorophyll fluorescence shows ecosystem-specific relationships to gross primary production: An assessment based on observational and modeling approaches. Remote Sens. Environ. 166, 91–105. https://doi.org/10.1016/j.rse.2015.06.004

Damm, A., Guanter, L., Verhoef, W., Schläpfer, D., Garbari, S., Schaepman, M.E., 2015. Impact of varying irradiance on vegetation indices and chlorophyll fluorescence derived from spectroscopy data. Remote Sens. Environ. 156, 202–215. https://doi.org/10.1016/j.rse.2014.09.031

Datt, B., 1998. Remote Sensing of Chlorophyll< i> a</i>, Chlorophyll< i> b</i>,

Chlorophyll< i> a</i>+< i> b</i>, and Total Carotenoid Content in Eucalyptus Leaves. Remote Sens. Environ. 66, 111–121.

Davidson, M., Berger, M., Moreno, J., Stoll, M., Miller, J., 2003. Photosynthesis from Space -.

Delang, C.O., Hang, Y.Y., 2010. Remote Sensing-Based Estimation of Carbon Sequestration in Hong Kong Country Parks from 1978 to 2004~!2009-05-13~!2009-09-17~!2009-12-30~! Open Environ. Sci. 3, 97–115. https://doi.org/10.2174/1876325100903010097

ESA-HYFLEX, 2013. Final Report Technical Assistance for the Deployment of an Advanced Hyperspectral Imaging Sensor during HYFLEX.

Frankenberg, C., Berry, J., Guanter, L., Joiner, J., 2013. Remote sensing of terrestrial chlorophyll fluorescence from space. SPIE Newsroom 2–5. https://doi.org/10.1117/2.1201302.004725

Frankenberg, C., Fisher, J.B., Worden, J., Badgley, G., Saatchi, S.S., Lee, J.-E., Toon, G.C., Butz, A., Jung, M., Kuze, A., Yokota, T., 2011. New global observations of the terrestrial carbon cycle from GOSAT: Patterns of plant fluorescence with gross primary productivity. Geophys. Res. Lett. 38, n/a-n/a. https://doi.org/10.1029/2011GL048738

Frankenberg, C., O'Dell, C., Guanter, L., McDuffie, J., 2012. Remote sensing of near-infrared chlorophyll fluorescence from space in scattering atmospheres: implications for its retrieval and interferences with atmospheric CO_2 retrievals. Atmos. Meas. Tech. 5, 2081–2094. https://doi.org/10.5194/amt-5-2081-2012

Gamon, a, Gamon, a, Serrano, L., Serrano, L., Surfus, S., Surfus, S., 1997. The

photochemical re¯ectance index: an optical indicator of photosynthetic radiation use ef®ciency across species, functional types, and nutrient levels. Oecologia 492–501.

Giardina, F., Konings, A.G., Kennedy, D., Alemohammad, S.H., Oliveira, R.S., Uriarte, M., Gentine, P., 2018. Tall Amazonian forests are less sensitive to precipitation variability. Nat. Geosci. 11, 405–409. https://doi.org/10.1038/s41561-018-0133-5

Guanter, L., Alonso, L., Gómez-Chova, L., Amorós-López, J., Vila, J., Moreno, J., 2007. Estimation of solar-induced vegetation fluorescence from space measurements. Geophys. Res. Lett. 34, L08401. https://doi.org/10.1029/2007GL029289

Guanter, L., Alonso, L., Gómez-Chova, L., Meroni, M., Preusker, R., Fischer, J., Moreno, J., 2010. Developments for vegetation fluorescence retrieval from spaceborne high-resolution spectrometry in the O2-A and O2-B absorption bands. J. Geophys. Res. Atmos. 115, 1–16. https://doi.org/10.1029/2009JD013716

He, L., Chen, J.M., Pan, Y., Birdsey, R., Kattge, J., 2012. Relationships between net primary productivity and forest stand age in U . S . forests 26, 1–19. https://doi.org/10.1029/2010GB003942

Homolová, L., Malenovský, Z., Clevers, J.G.P.W., García-Santos, G., Schaepman, M.E., 2013. Review of optical-based remote sensing for plant trait mapping. Ecol. Complex. 15, 1–16. https://doi.org/10.1016/j.ecocom.2013.06.003

Hong Kong Observatory, 2017. Climate of Hong Kong [WWW Document]. URL https://www.weather.gov.hk/cis/climahk_e.htm (accessed 1.1.19).

Jensen, J.R., 2007. Remote sensing of the environment : an earth resource perspective. Pearson Prentice Hall.

Jeong, S.-J., Schimel, D., Frankenberg, C., Drewry, D.T., Fisher, J.B., Verma, M., Berry,

J.A., Lee, J.-E., Joiner, J., 2017. Application of satellite solar-induced chlorophyll fluorescence to understanding large-scale variations in vegetation phenology and function over northern high latitude forests. Remote Sens. Environ. 190, 178–187. https://doi.org/10.1016/j.rse.2016.11.021

Joiner, J., Guanter, L., Lindstrot, R., Voigt, M., Vasilkov, a. P., Middleton, E.M., Huemmrich, K.F., Yoshida, Y., Frankenberg, C., 2013. Global monitoring of terrestrial chlorophyll fluorescence from moderate spectral resolution near-infrared satellite measurements: methodology, simulations, and application to GOME-2. Atmos. Meas. Tech. Discuss. 6, 3883–3930. https://doi.org/10.5194/amtd-6-3883-2013

Joiner, J., Yoshida, Y., Vasilkov, a. P., Corp, L. a., Middleton, E.M., 2011. First observations of global and seasonal terrestrial chlorophyll fluorescence from space. Biogeosciences 8, 637–651. https://doi.org/10.5194/bg-8-637-2011

Julitta, T., Corp, L.A., Rossini, M., Burkart, A., Cogliati, S., Davies, N., Hom, M., Arthur, A. Mac, Middleton, E.M., Rascher, U., Schickling, A., Colombo, R., 2016. Comparison of sun-induced chlorophyll fluorescence estimates obtained from four portable field spectroradiometers. Remote Sens. 8, 1–14. https://doi.org/10.3390/rs8020122

Kaufmann, H., Segl, K., Itzerott, S., Bach, H., Wagner, a., Hill, J., Heim, B., Oppermann, K., Heldens, W., Stein, E., Müller, a., van der Linden, S., Leitão, P.J., Rabe, a., Hostert, P., 2010. Hyperspectral algorithms: report in the frame of EnMAP preparation activities 268. https://doi.org/http://doi.org/10.2312/GFZ.b103-10089

Khosravi, N., 2012. M . Sc . Thesis Terrestrial Plant Fluorescence as seen from Satellite

Data.

Krause, G.H., Weis, E., 1991. Chlorophyll Fluorescence and Photosynthesis: The Basics. Annu. Rev. Plant Physiol. Plant Mol. Biol. 42, 313–349. https://doi.org/10.1146/annurev.pp.42.060191.001525

Maeir. W Stefan, Gunther. P Kurt, S.M., 2003. Maeir et al 2003 - Sun Induced Fluorescence A New Tool for Precision Farming.

Maier, S.W., Günther, K.P., Stellmes, M., 2003. Sun-induced fluorescence: a new tool for precision farming. Digit. Imaging Spectr. Tech. Appl. to Precis. Agric. Crop Physiol. 209–222.

Mazzoni, M., Falorni, P., Verhoef, W., 2010. High-resolution methods for fluorescence retrieval from space. Opt. Express 18, 15649–63.

Meroni, M., Busetto, L., Colombo, R., Guanter, L., Moreno, J., Verhoef, W., 2010. Performance of Spectral Fitting Methods for vegetation fluorescence quantification. Remote Sens. Environ. 114, 363–374. https://doi.org/10.1016/j.rse.2009.09.010

Meroni, M., Colombo, R., 2006. Leaf level detection of solar induced chlorophyll fluorescence by means of a subnanometer resolution spectroradiometer. Remote Sens. Environ. 103, 438–448. https://doi.org/10.1016/j.rse.2006.03.016

Meroni, Michele, Panigada, C., Rossini, M., Picchi, V., Cogliati, S., Colombo, R., 2009. Using optical remote sensing techniques to track the development of ozone-induced stress. Environ. Pollut. 157, 1413–20. https://doi.org/10.1016/j.envpol.2008.09.018

Meroni, M., Rossini, M., Guanter, L., Alonso, L., Rascher, U., Colombo, R., Moreno, J., 2009. Remote sensing of solar-induced chlorophyll fluorescence: Review of methods and applications. Remote Sens. Environ. 113, 2037–2051.

https://doi.org/10.1016/j.rse.2009.05.003

Migliavacca, M., Perez-Priego, O., Rossini, M., El-Madany, T.S., Moreno, G., van der Tol, C., Rascher, U., Berninger, A., Bessenbacher, V., Burkart, A., Carrara, A., Fava, F., Guan, J.H., Hammer, T.W., Henkel, K., Juarez-Alcalde, E., Julitta, T., Kolle, O., Martín, M.P., Musavi, T., Pacheco-Labrador, J., Pérez-Burgueño, A., Wutzler, T., Zaehle, S., Reichstein, M., 2017. Plant functional traits and canopy structure control the relationship between photosynthetic CO2 uptake and far-red sun-induced fluorescence in a Mediterranean grassland under different nutrient availability. New Phytol. 214, 1078–1091. https://doi.org/10.1111/nph.14437

Montagna, M., 2008. Brillouin and Raman scattering from the acoustic vibrations of spherical particles with a size comparable to the wavelength of the light. Phys. Rev. B - Condens. Matter Mater. Phys. 77, 1–9. https://doi.org/10.1103/PhysRevB.77.045418

Moreno, J.F., Asner, G.P., Bach, H., Belenguer, T., Bell, A., Buschmann, C., Calera, A., Calpe, J., Campbell, P., Cecchi, G., Colombo, R., Corp, L. a, Court, A., 2006. FLuorescence EXplorer (FLEX): mapping vegetation photosynthesis from space 832–837.

Moya et al 1995 - Remote Sensing of time resolve chlorophyl flourescence of excitation of laser by vegetation.pdf, n.d.

Moya, I., 2004. A new instrument for passive remote sensing1. Measurements of sunlight-induced chlorophyll fluorescence. Remote Sens. Environ. 91, 186–197. https://doi.org/10.1016/j.rse.2004.02.012

Nazeer, M., Nichol, J.E., Yung, Y., 2014. Evaluation of atmospheric correction models

and Landsat surface reflectance product in an urban coastal environment. Int. J. Remote Sens. 37–41. https://doi.org/10.1080/01431161.2014.951742

Ni, Z., Liu, Z., Li, Z.-L., Nerry, F., Huo, H., Li, X., 2015. Estimation of solar-induced fluorescence using the canopy reflectance index. Int. J. Remote Sens. 1–18. https://doi.org/10.1080/01431161.2015.1058987

Ni, Z., Liu, Z., Li, Z.L., Nerry, F., Huo, H., Sun, R., Yang, P., Zhang, W., 2016. Investigation of atmospheric effects on retrieval of sun-induced fluorescence using hyperspectral imagery. Sensors (Switzerland) 16. https://doi.org/10.3390/s16040480

Niinemets, Ü., 2010. Responses of forest trees to single and multiple environmental stresses from seedlings to mature plants: Past stress history, stress interactions, tolerance and acclimation. For. Ecol. Manage. 260, 1623–1639. https://doi.org/10.1016/j.foreco.2010.07.054

Panigada, C., Colombo, R., Meroni, M., Rossini, M., Cogliati, S., Busetto, L., Fava, F., Picchi, V., Migliavacca, M., Marchesi, A., 2010. REMOTE SENSING OF VEGETATION STATUS USING 2010, 17–19.

Perez-Priego, O., Guan, J., Rossini, M., Fava, F., Wutzler, T., Moreno, G., Carvalhais, N., Carrara, A., Kolle, O., Julitta, T., Schrumpf, M., Reichstein, M., Migliavacca, M., 2015. Sun-induced chlorophyll fluorescence and photochemical reflectance index improve remote-sensing gross primary production estimates under varying nutrient availability in a typical Mediterranean savanna ecosystem. Biogeosciences 12, 6351–6367. https://doi.org/10.5194/bg-12-6351-2015

Planet labs, 2016. Planet imagery specifications. San Francisco, CA.

Plascyk, J., 1975. The MK II Fraunhofer Line Discriminator (FLD-II) The MK II

Fraunhofer Line Discriminator (FLD -II) for Airborne and Orbital Remote Sensing of Solar-Stimulated Luminescence. Opt. Eng. 14, 339–346. https://doi.org/10.1117/12.7971842

Plascyk, J.A., 1975. <title>The MK II Fraunhofer Line Discriminator (FLD-II) for Airborne and Orbital Remote Sensing of Solar-Stimulated Luminescence</title>. Opt. Eng. 14, 339. https://doi.org/10.1117/12.7971842

Platt, U., 2017. Air Monitoring by Differential Optical Absorption Spectroscopy. Encycl. Anal. Chem. 1–28. https://doi.org/10.1002/9780470027318.a0706.pub2

Porcar-Castell, A., Tyystjärvi, E., Atherton, J., van der Tol, C., Flexas, J., Pfündel, E.E., Moreno, J., Frankenberg, C., Berry, J. a, 2014. Linking chlorophyll a fluorescence to photosynthesis for remote sensing applications: mechanisms and challenges. J. Exp. Bot. 65, 4065–95. https://doi.org/10.1093/jxb/eru191

RAMSES-ARC, 2016. RAMSES-ARC RAMSES-ARC. Oldenburg, Germany.

Ranjan S. Muttiah, 2002. From Laboratory Spectroscopy to Remotely Sensed Spectra of Terrestrial Ecosystems. Springer Netherlands, Dordrecht. https://doi.org/10.1007/978-94-017-1620-8

Rascher, U., Alonso, L., Burkart, a., Cilia, C., Cogliati, S., Colombo, R., Damm, a., Drusch, M., Guanter, L., Hanus, J., Hyvärinen, T., Julitta, T., Jussila, J., Kataja, K., Kokkalis, P., Kraft, S., Kraska, T., Matveeva, M., Moreno, J., Muller, O., Panigada, C., Pikl, M., Pinto, F., Prey, L., Pude, R., Rossini, M., Schickling, a., Schurr, U., Schüttemeyer, D., Verrelst, J., Zemek, F., 2015. Sun-induced fluorescence - a new probe of photosynthesis: First maps from the imaging spectrometer *HyPlant*. Glob. Chang. Biol. n/a-n/a. https://doi.org/10.1111/gcb.13017

Raychaudhuri, B., 2014a. Solar-induced fluorescence of terrestrial chlorophyll derived from the O 2 -A band of Hyperion hyperspectral images. Remote Sens. Lett. 5, 941–950. https://doi.org/10.1080/2150704X.2014.976884

Raychaudhuri, B., 2014b. Solar-induced fluorescence of terrestrial chlorophyll derived from the O 2 -A band of Hyperion hyperspectral images. Remote Sens. Lett. 5, 941–950. https://doi.org/10.1080/2150704X.2014.976884

Rossini, M., Alonso, L., Cogliati, S., Damm, A., Guanter, L., Julitta, T., Meroni, M., Moreno, J., Panigada, C., Pinto, F., Rascher, U., Schickling, A., Schüttemeyer, D., Zemek, F., Colombo, R., 2014. Measuring Sun-Induced Chlorophyll Fluorescence : an Evaluation and Synthesis of Existing Field Data. 5th Int. Work. Remote Sens. Veg. Fluoresc. 8–12.

Rouse, J. W., Jr., Haas, R. H., Schell, J. A., Deering, D. W., 1974. Monitoring Vegetation Systems in the Great Plains with Erts. Third Earth Resour. Technol. Satell. Symp. Vol. I Tech. Present. NASA SP-351.

Ryan, M.G., Binkley, D., Fownes, J.H., 1997. Age-Related Decline in Forest Productivity: Pattern and Process, in: Begon, M., Fitter, A.H.B.T.-A. in E.R. (Eds.), . Academic Press, pp. 213–262. https://doi.org/https://doi.org/10.1016/S0065-2504(08)60009-4

Staenz, K., Neville, R. a., Clavette, S., Landry, R., White, H.P., Hitchcock, R., n.d. Retrieval of surface reflectance from Hyperion radiance data. IEEE Int. Geosci. Remote Sens. Symp. 3, 1419–1421. https://doi.org/10.1109/IGARSS.2002.1026135

Tol, C. Van Der, Berry, J. a, Campbell, P.K.E., Rascher, U., 2014. Models of fluorescence and photosynthesis for interpreting measurements of solar-induced chlorophyll

fluorescence 1–16. https://doi.org/10.1002/2014JG002713.We

Wang, J., Wang, T., Skidmore, A., Shi, T., Wu, G., 2015. Evaluating Different Methods for Grass Nutrient Estimation from Canopy Hyperspectral Reflectance. Remote Sens. 7, 5901–5917. https://doi.org/10.3390/rs70505901

Wolanin, a., Rozanov, V.V., Dinter, T., Noël, S., Vountas, M., Burrows, J.P., Bracher, a., 2015. Global retrieval of marine and terrestrial chlorophyll fluorescence at its red peak using hyperspectral top of atmosphere radiance measurements: Feasibility study and first results. Remote Sens. Environ. 166, 243–261. https://doi.org/10.1016/j.rse.2015.05.018

Zarco-Tejada, P.., Pushnik, J.., Dobrowski, S., Ustin, S.., 2003. Steady-state chlorophyll a fluorescence detection from canopy derivative reflectance and double-peak red-edge effects. Remote Sens. Environ. 84, 283–294. https://doi.org/10.1016/S0034-4257(02)00113-X

Zarco-tejada, P.J., Miller, J.R., Mohammed, G.H., Noland, T.L., 2000. Chlorophyll Fluorescence Effects on Vegetation Apparent Reflectance : I . Leaf-Level Measurements and Model Simulation 595, 582–595.

Zhang, M., Li, G., Wang, S., Fu, Z., Guan, Y., Lin, L., 2017. The influence of different integration time on stoichiometric analysis in near infrared grating spectrometers. Infrared Phys. Technol. 86, 130–134. https://doi.org/10.1016/j.infrared.2017.08.018

Zhang, Q., Middleton, E.M., Cheng, Y. Ben, Huemmrich, K.F., Cook, B.D., Corp, L.A., Kustas, W.P., Russ, A.L., Prueger, J.H., Yao, T., 2016. Integrating chlorophyll fAPAR and nadir photochemical reflectance index from EO-1/Hyperion to predict cornfield daily gross primary production. Remote Sens. Environ. 186, 311–321.

https://doi.org/10.1016/j.rse.2016.08.026

Zhang, Y., Guanter, L., Berry, J. a, Joiner, J., van der Tol, C., Huete, A., Gitelson, A., Voigt, M., Köhler, P., 2014. Estimation of vegetation photosynthetic capacity from space-based measurements of chlorophyll fluorescence for terrestrial biosphere models. Glob. Chang. Biol. 1–16. https://doi.org/10.1111/gcb.12664

Zhou, T., Shi, P., Jia, G., Dai, Y., Zhao, X., Shangguan, W., Du, L., Wu, H., Luo, Y., 2015. Age-dependent forest carbon sink: Estimation via inverse modeling 2473–2492. https://doi.org/10.1002/2015JG002943.Received